Lymphotoxin beta receptor-/- mice display altered B- and T-cell subpopulations in the bone marrow and peritoneal cavity after Toxoplasma gondii infection

Marcel Helle, Ursula R. Sorg, Johannes Ptok, Rachel E. Thomas, Katharina Pracht, Patrick Petzsch, Alain de Bruin, Hans-Martin Jäck, Karl Köhrer, Daniel Degrandi, Klaus Pfeffer

AMERICAN SOCIETY FOR MICROBIOLOGY | Infection and Immunity

| Immunology | Full-Length Text

Lymphotoxin beta receptor$^{-/-}$ mice display altered B- and T-cell subpopulations in the bone marrow and peritoneal cavity after *Toxoplasma gondii* infection

Marcel Helle,[1] Ursula R. Sorg,[1] Johannes Ptok,[2] Rachel E. Thomas,[3] Katharina Pracht,[4] Patrick Petzsch,[5] Alain de Bruin,[3] Hans-Martin Jäck,[4] Karl Köhrer,[5] Daniel Degrandi,[1] Klaus Pfeffer[6]

AUTHOR AFFILIATIONS See affiliation list on p. 19.

ABSTRACT Lymphotoxin β receptor (LTβR/TNFRSF3) signaling plays a crucial role in immune defense. Notably, LTβR-deficient (LTβR$^{-/-}$) mice exhibit severe defects in innate and adaptive immunity against various pathogens and succumb to *Toxoplasma gondii* infection. Here, we investigated the bone marrow (BM) and peritoneal cavity (PerC) compartments of LTβR$^{-/-}$ mice during *T. gondii* infection, demonstrating perturbed B-cell and T-cell subpopulations in the absence of LTβR signaling. *T. gondii* infection disrupted BM lymphopoiesis, depleting early and mature B cells in WT mice, whereas mature B cells remained present in LTβR$^{-/-}$ BM. LTβR$^{-/-}$ BM also exhibited reduced MHCII^{+} monocytes and a plasma cell compartment skewed toward IgM^{+} rather than IgA^{+} cells. In addition, BM Tcell subsets were altered, exhibiting decreased double-negative (CD4^{-}/CD8^{-}) and increased CD4^{+} and CD8^{+} T-cell frequencies. Analysis of the BM transcriptome revealed diminished interferon responses but an upregulated TNFα-NF-κB signaling signature in uninfected and infected LTβR$^{-/-}$ mice, potentially compensating for the absence of LTβR signaling. LTβR$^{-/-}$ mice displayed an altered B-1a to B-1b ratio and a predominant presence of neutrophils in the PerC. In summary, we identified novel immunological alterations in the BM and PerC compartments of LTβR$^{-/-}$ mice, which suggest new roles for LTβR signaling in B- and T-cell homeostasis, migration, and pathogen defense.

KEYWORDS lymphotoxin beta receptor, *Toxoplasma gondii*, adaptive immunity, B cells, bone marrow, peritoneal cavity, B-1 cells

The LTβR (TNFRSF3) is a member of the tumor necrosis factor receptor superfamily (TNFRSF) and is expressed by a wide variety of cell types including epithelial, endothelial, stromal, and myeloid cells (e.g., monocytes, macrophages [1, 2], neutrophils [1, 3], dendritic cells [DCs; 4–6], and mast cells), but is absent from lymphoid cells (7, 8). Conversely, the two known LTβR ligands, $LT\alpha_1\beta_2$ and LIGHT (**l**ymphotoxin-like, exhibits **i**nducible expression, and competes with HSV **g**lycoprotein D for **h**erpesvirus entry mediator, a receptor expressed by **T** lymphocytes), are expressed on lymphoid cells, suggesting that LTβR signaling mainly occurs in a paracrine or juxtacrine manner (7, 8). While the lymphotoxin heterotrimer $LT\alpha_1\beta_2$ is LTβR-specific, the second ligand LIGHT can also bind two other TNFRSF members: herpes virus entry mediator (HVEM) and soluble decoy receptor 3 (DcR3) (7–9). LTβR-induced downstream signaling occurs primarily via the canonical and the alternative nuclear factor "kappa-light-chain-enhancer" of activated B-cell (NF-κB) pathways (8, 10).

The LTβR is essential for the development of lymphoid organs during embryogenesis and for structural maintenance of lymphoid organs as well as immune cell homeostasis in adulthood (11–13). LTβR-deficient mice (LTβR$^{-/-}$) lack lymph nodes (LN) and Peyer's Patches (PPs) (11), and exhibit an altered splenic microenvironment characterized by

Editor Jeroen P. J. Saeij, University of California Davis, Davis, California, USA

Address correspondence to Klaus Pfeffer, klaus.pfeffer@hhu.de, or Marcel Helle, Marcel.Helle@uni-duesseldorf.de.

The authors declare no conflict of interest.

See the funding table on p. 20.

Received 6 August 2025
Accepted 12 August 2025
Published 9 September 2025

disrupted B- and T-cell compartmentalization (14, 15), germinal center (GC) formation (16, 17), and markedly reduced numbers of follicular DCs (FDCs) (5, 13, 18, 19), macrophages (11, 13, 20, 21), natural killer (NK), and NKT cells (13, 22–25). Another affected organ is the thymus, where LTβR signaling is involved in thymocyte migration and the establishment of central tolerance (26). In addition, LTβR$^{-/-}$ mice exhibit signs of autoimmunity, including splenomegaly, increased perivascular lymphocytic infiltrations of non-lymphoid organs, autoantibody production, and increased baseline immune activation (11, 13, 25, 27–29). Furthermore, the well-documented inability of LTβR$^{-/-}$ mice to mount adequate immune responses against various pathogens underscores its critical role for immunity (13, 25, 29–34). Consequently, there has been growing interest in exploring the role of LTβR signaling in infection, autoimmune diseases, and cancer (35–38).

Toxoplasma gondii is an obligate intracellular protozoan parasite that belongs to the phylum Apicomplexa. *T. gondii* can infect virtually all warm-blooded vertebrates, including humans. This successful parasite has infected 30%–50% of the world's human population (39) and can persist lifelong in the host (40, 41). While *T. gondii* infection usually causes mild, flu-like symptoms in immunocompetent hosts, an infection of immunocompromised individuals or congenitally infected unborn children can lead to diverse and severe health issues, including encephalitis, myocarditis, pneumonia, and abortion (42). No vaccine is currently available against *T. gondii* (43).

The host immune response against *T. gondii* requires a coordinated interplay of innate, adaptive, and cell-autonomous immunity (44–47). *T. gondii* infection stimulates a proinflammatory cascade resulting in massive interferon-gamma (IFNγ) production by NK cells (48, 49), CD4$^+$ and CD8$^+$ T cells (48, 50–52), and innate lymphoid type I cells (ILC1s) (53–56). An early and potent production of IFNγ is essential for effective parasite control (57, 58). IFNγ (further) activates immune cells such as monocytes, macrophages, DCs, NK, and T cells, and it induces the expression of hundreds of genes involved in cell-autonomous immunity to inhibit intracellular pathogens (47). This includes the direct targeting and destruction of *T. gondii* and its surrounding parasitophorous vacuole (PV) by immunity-related GTPases (IRGs) (59–63) and guanylate-binding proteins (GBPs) (64–68). However, while a strong T-helper 1 (Th1) response driven by IL-12 and IFNγ is necessary for effective parasite restriction, it can also trigger severe immunopathology in the host (69–74).

In addition to classic CD4$^+$ and CD8$^+$ T-cell populations, double-negative (DN; CD4$^-$/CD8$^-$) T cells lack both CD4 and CD8 co-receptors and can be found as a rare T-cell subpopulation in the periphery (1%–5% of CD3$^+$ T cells) (75, 76). They are enriched in the bone marrow (BM), where they constitute up to one-third of CD3$^+$ T cells (77). While details remain elusive, the heterogeneous DN T cells can be of thymic or extrathymic origin and exert proinflammatory as well as immunosuppressive effects (78). Their potential role in immune responses, disease, and therapy has increasingly gained recognition (78–81).

B cells and antibody-mediated immunity further contribute to host defense against *T. gondii* infection (82–89). However, there are major differences between B-cell subpopulations. B-1 cells are mainly of fetal origin and have self-renewing capacities, whereas conventional (B-2) cells need to be continuously generated from progenitors in the adult BM (90). Most B-2 cells leave the BM at the transitional stage and complete their maturation in secondary lymphatic organs like the spleen, from where they may circulate through the bloodstream and re-enter the BM as recirculating mature B cells (91, 92). While B-1 cells are a rare subpopulation in the BM, peripheral blood (PB), spleen, and lymph nodes (0.1%–2% of CD19$^+$ B cells), they are enriched in body cavities such as the peritoneal and pleural cavities (35%–70% of CD19$^+$ B cells) (93). They are considered innate-like B cells due to their more restricted B-cell receptor repertoire, their role as the major source of natural antibodies, and their capability of rapid, mainly T-cell-independent secretion of low-affinity IgM during early infection (94–99). Depending on the cell surface expression of CD5, B-1 cells are further divided into B-1a (CD5$^+$) cells, which are

considered the main natural antibody producers, and B-1b ($CD5^-$) cells, which are more involved in the adaptive antibody response than B-1a cells (96). While B-1 cells have been shown to contribute to protection against *T. gondii* alongside conventional B-2 cells (86, 89), they are also a predisposed source of autoantibodies induced by *T. gondii* infection and can negatively impact host defense (100, 101). However, the interplay between protozoan parasites and the B-cell response is diverse and not fully understood (102–105).

In our previous studies, we showed that $LT\beta R^{-/-}$ mice are highly susceptible and rapidly succumb to *T. gondii* (25, 29). The expression of IFNγ and downstream effector molecules, such as mGBPs, was significantly delayed. Adaptive immunity of $LT\beta R^{-/-}$ mice was also affected, as evidenced by reduced secretion of IFNγ by $CD4^+$ T cells and cytotoxic granules by $CD8^+$ T cells after *ex vivo* stimulation (25). B cells in the spleen of WT mice were significantly reduced during *T. gondii* infection, but this reduction was attenuated in $LT\beta R^{-/-}$ mice. In addition, $LT\beta R^{-/-}$ mice showed only low amounts of parasite-specific IgM in the serum, whereas parasite-specific immunoglobulin heavy-chain class-switching and IgG production were abrogated (25).

Here, we expand and deepen our investigation of the B-cell immune response and B-cell subpopulations to the BM and peritoneal cavity (PerC) of $LT\beta R^{-/-}$ mice and demonstrate its intriguing dynamics during *T. gondii* infection. A striking phenotype of the $LT\beta R^{-/-}$ BM was increased mature B-cell frequencies, which displayed a unique resistance to inflammation-induced reduction compared to WT mature B cells. While $MHCII^+$ proinflammatory monocytes were diminished in $LT\beta R^{-/-}$ compared to WT BM, plasma cell (PC) frequencies were comparable or even increased; however, the majority of $LT\beta R^{-/-}$ bone marrow PCs (BMPCs) displayed surface IgM rather than IgA, in contrast to WT BMPCs. In addition, we found that T-cell subset frequencies were altered in the BM of $LT\beta R^{-/-}$ mice, with decreased DN T cell and increased $CD4^+$ and $CD8^+$ T cell frequencies. RNA sequencing revealed significantly reduced interferon-related gene sets and an enriched "TNFα-signaling via NF-κB" gene set in $LT\beta R^{-/-}$ BM compared to WT BM prior to and after *T. gondii* infection. In the $LT\beta R^{-/-}$ PerC, B-2 and B-1b cell frequencies were increased, whereas B-1a frequencies were comparable to WT counterparts, leading to altered B-1a to B-1b ratios in $LT\beta R^{-/-}$ mice. Finally, the predominant presence of neutrophils over T cells in the $LT\beta R^{-/-}$ PerC on day 9 p.i. marks a profound difference, showing that parasite replication is not effectively inhibited despite neutrophil accumulation, which likely contributed to exacerbated immunopathology. These results will hopefully enhance our understanding of the role of LTβR signaling in immune cell homeostasis and during intracellular parasite infections.

RESULTS

Mature B cells are increased in the BM of $LT\beta R^{-/-}$ mice and show less severe reduction during *T. gondii* infection

WT and $LT\beta R^{-/-}$ mice were intraperitoneally (i.p.) infected with *T. gondii* (ME49) and analyzed on days 3, 6, and 9 p.i. In the BM, *T. gondii* burden increased over the course of infection; on day 9 p.i., $LT\beta R^{-/-}$ mice showed significantly increased *T. gondii* numbers (>20-fold) as compared to WT mice (Fig. 1a). At the same time, total leukocyte numbers per femur did not significantly differ or change between genotypes over the course of *T. gondii* infection (Fig. 1b). Interestingly, $CD19^+$ $B220^+$ pan-B cells were already significantly increased in $LT\beta R^{-/-}$ BM before infection compared to WT BM (Fig. 1c and d; for gating strategy see Fig. S1, for absolute cell numbers see S2a). But while pan-B-cell frequencies were found significantly reduced in WT BM by day 6 p.i., they remained stable in $LT\beta R^{-/-}$ BM at this point (Fig. 1c and d). Both genotypes showed a significant reduction of pan-B cells from day 6 to day 9 p.i. However, the overall pan-B-cell reduction was much less severe in $LT\beta R^{-/-}$ mice (−61.0% on day 9 p.i. compared to uninfected) compared to WT mice (−95.7% on day 9 p.i. compared to uninfected), mirroring the course of splenic B-cell frequencies after *T. gondii* infection as described previously (25).

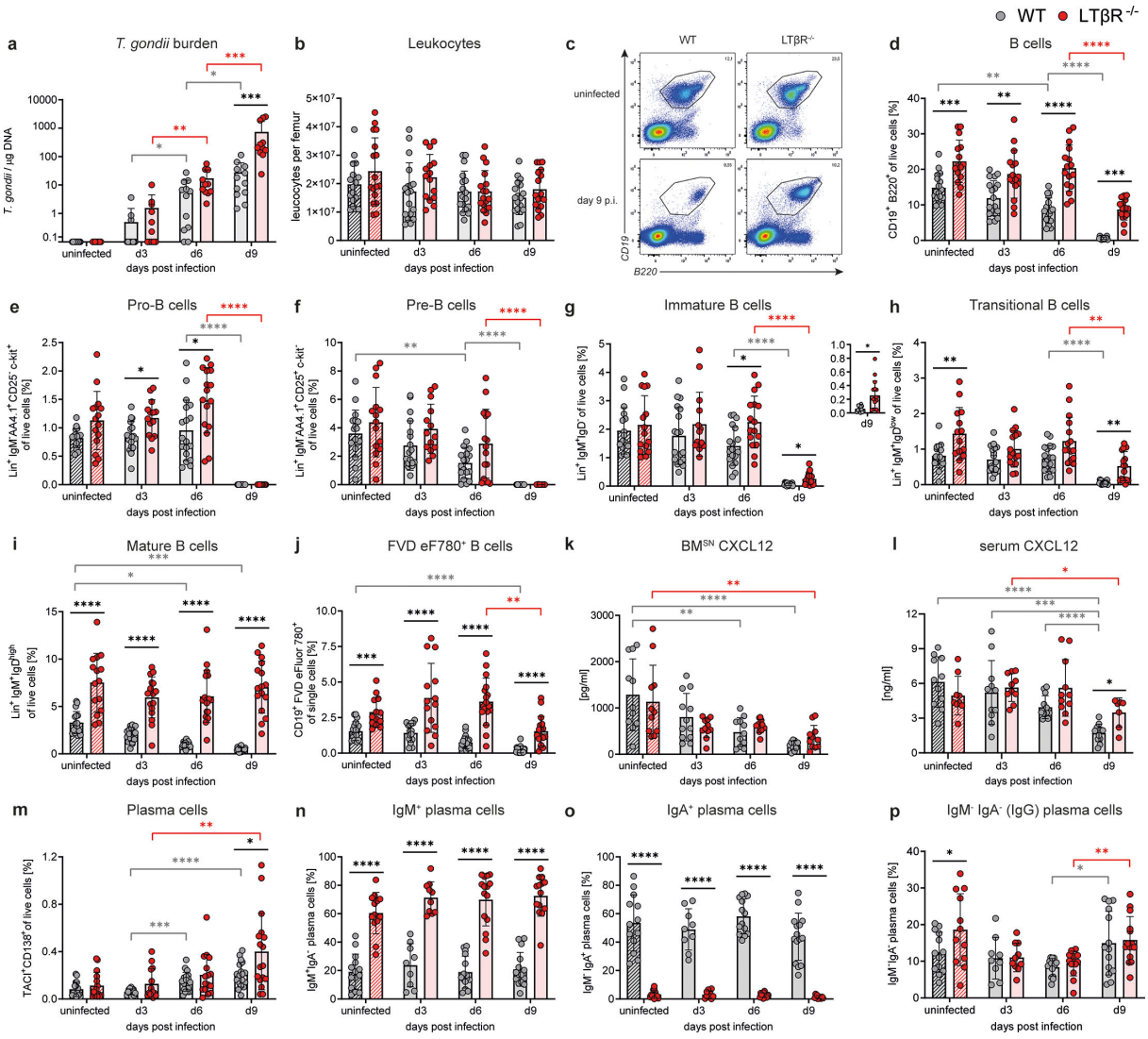

FIG 1 Altered B-cell subpopulations and CXCL12 concentrations in the BM of *T. gondii*-infected WT and LTβR$^{-/-}$ mice. (a) DNA was isolated from the BM and used to assess the *T. gondii* burden via quantitative real-time PCR of the B-1 gene (*TgB1*). A standard curve generated from a defined number of ME49 tachyzoites (2914 ± 214 /µL) was used to calculate parasite loads in WT ($n \geq 10$/group) and LTβR$^{-/-}$ ($n \geq 8$/group) mice. (b) Counted leukocytes per femur from uninfected and infected WT ($n \geq 17$/group) and LTβR$^{-/-}$ ($n \geq 15$/group) mice. Using surface marker staining and flow cytometry (gating strategy: Fig. S1), the following immune cell populations in the BM of WT ($n \geq 15$/group) and LTβR$^{-/-}$ ($n \geq 13$/group) mice were identified and quantified as percentages of live cells, unless otherwise specified: (c and d) Pan-B cells (CD19$^+$ B220$^+$) (c) shows a set of representative images. (c–i) Lin$^+$ = CD19$^+$ B220$^+$. (e) Pro-B cells (Lin$^+$ IgM$^-$ AA4.1$^+$ CD25$^-$ c-kit$^+$), (f) Pre-B cells (Lin$^+$ IgM$^-$ AA4.1$^+$ CD25$^+$ c-kit$^-$), (g) Immature B cells (Lin$^+$ IgM$^+$ IgD$^-$), (h) Transitional B cells (Lin$^+$ IgM$^+$ IgD^{low}), and (i) Mature B cells (Lin$^+$ IgM$^+$ IgD^{high}). (j) Dead B cells (CD19$^+$ FVD eFluor780$^+$), % of single cells. (k and l) CXCL12 measured in the (k) BM^{SN} and (l) serum of uninfected and infected WT ($n \geq 10$/group) and LTβR$^{-/-}$ ($n \geq 7$/group) mice via bead-based immunoassay (LegendPlex, BioLegend, USA). (**m**) BMPCs (TACI$^+$ CD138$^+$). WT: $n \geq 13$/group, LTβR$^{-/-}$: $n \geq 14$/group. (n–p) IgM$^+$, IgA$^+$, and IgM$^-$ IgA$^-$ (IgG) expressing PCs (surface Ig), % of BMPCs. WT: $n \geq 9$/group, LTβR$^{-/-}$: $n \geq 10$/group. All data shown represent at least four independent experiments; symbols represent individual animals and columns represent means ± SD. *$P < 0.05$; **$P < 0.01$; ***$P < 0.001$; ****$P < 0.0001$.

To identify which B-cell subpopulation(s) was responsible for the increased B-cell numbers in the LTβR$^{-/-}$ BM, B-cell developmental stages were investigated based on surface marker expression (Fig. S1; Table S1 and S2). Pro-, pre-, and immature B-cell populations were mostly comparable between genotypes (Fig. 1e through g; Fig. S2b through d), while transitional B-cell (Lin$^+$ IgM$^+$ IgD^{low}, Fig. 1H; Fig. S2e) frequencies were increased in uninfected LTβR$^{-/-}$ mice and on day 9 p.i. Notably, mature B cells (Lin$^+$ IgM$^+$

IgD^{high}) were the primary contributors to the increased BM B-cell population in LTβR$^{-/-}$ mice, as they were significantly increased at all examined time points compared to their WT BM counterparts (Fig. 1i; Fig. S2f).

The strong reduction of B cells on day 9 p.i. was observed across all investigated B-cell subpopulations in WT BM (Fig. 1e through i; Fig. S2b through f). But while this was also evident in early-stage B-cell populations in LTβR$^{-/-}$ BM, the transitional and mature B cells were notable exceptions. More precisely, on day 9 p.i., pro-, pre-, and immature B cells were nearly absent in both WT and LTβR$^{-/-}$ BM (Fig. 1e through g; Fig. S2b through d). However, while transitional B cells in LTβR$^{-/-}$ mice were significantly reduced on day 9 compared to day 6 p.i., they were significantly increased compared to WT on day 9 p.i. (Fig. 1h; Fig. S2e). Mature B cells remained unaffected in LTβR$^{-/-}$ BM during infection and were therefore highly significantly increased compared to the WT at all time points during infection (Fig. 1i; Fig. S2f). These results demonstrate that both phenotypes observed in the LTβR$^{-/-}$ BM - the increased B cells under steady-state conditions and the enhanced resistance to reduction during *T. gondii* infection - are specific to particular late-stage B-cell populations, with mature B cells exhibiting the most significant alterations.

To investigate whether the reduction of B cells on day 9 p.i. was caused by B-cell death or by mobilization and egress, we used a viability dye (FVD eF780) to detect dead cells (Fig. S1; Table S1 and S2). LTβR$^{-/-}$ mice had significantly increased frequencies of dead B cells in the BM before and during *T. gondii* infection (Fig. 1j), even though both genotypes showed comparable frequencies of dead BM leukocytes (Fig. S2g). On day 9 p.i., frequencies of dead B cells were lower compared to previous days, possibly due to the overall reduced presence of B cells on that day in both genotypes (Fig. 1j). Similar to the results described for living cells, dead early B cells (FVD eF780$^+$ CD19$^+$ AA4.1$^+$ IgM$^-$) were almost completely absent on day 9 p.i. in both WT and LTβR$^{-/-}$ animals (Fig. S2h), while dead mature B cells (FVD eF780$^+$ CD19$^+$ IgM$^+$ IgD$^+$) were significantly increased in LTβR$^{-/-}$ animals (Fig. S2i).

The chemokine C-X-C motif chemokine 12 (CXCL12) is, among other functions, essential for hematopoiesis and regulating B-cell development by directing them to and retaining them in specific BM niches (106). During inflammation, a reduction of CXCL12 in the BM has been shown to lead to the mobilization and egress of B-cell precursors (107). CXCL12 concentrations were therefore determined in the BM supernatant (BM^{SN}) and serum of WT and LTβR$^{-/-}$ mice. CXCL12 concentrations declined during *T. gondii* infection and were significantly reduced in the BM^{SN} (Fig. 1k) and serum (Fig. 1l) on day 9 p.i. in WT and LTβR$^{-/-}$ mice. While the decrease in BM^{SN} CXCL12 after infection likely explains the egress of early B-cell populations and thus the almost complete loss of pro- and pre-B cells observed on day 9 p.i., early B cells (AA4.1$^+$) were decreased, rather than increased, in the PB on day 9 p.i. (Fig. S3a). Instead, a significantly increased AA4.1-positive myeloid (CD11b$^+$) population was identified in the PB of both genotypes (Fig. S3b and c). Overall, LTβR$^{-/-}$ mice showed higher numbers of circulating PB leukocytes (Fig. S3d) and increased frequencies of PB (mature) B cells (Fig. S3e and f) compared to WT controls. In contrast to the unaffected frequencies of mature B cells in the LTβR$^{-/-}$ BM, their frequency in the PB was reduced on day 9 p.i. but was still significantly higher than in WT animals (Fig. S3f).

In contrast to CXCL12, concentrations of B-cell activating factor (BAFF), another cytokine important for B-cell development, remained stable in the BM^{SN} (Fig. S4a) and increased in the serum (Fig. S4b) over the course of infection. However, BAFF concentrations were always comparable between WT and LTβR$^{-/-}$ mice.

Surprisingly, despite lacking lymph nodes, PPs (11), and GC reactions (13, 17), LTβR$^{-/-}$ mice had equal or increased (day 9 p.i.) frequencies of BMPCs (TACI$^+$ CD138$^+$ [108]) compared to WT mice (Fig. 1m, Fig. S4c and d), the origin of which remains unclear. However, the majority of LTβR$^{-/-}$ BMPCs were surface IgM positive, which is in contrast to the predominantly IgA-positive WT BMPCs (Fig. 1n and o; Fig. S4e and g). Double-neg-

ative (IgM^- IgA^-), presumably IgG^+, BMPC frequencies were elevated in uninfected $LT\beta R^{-/-}$ mice but otherwise comparable between genotypes (Fig. 1p; Fig. S4h).

In summary, the $LT\beta R^{-/-}$ BM contained significantly increased frequencies of mature B cells under steady-state conditions, which were also more resistant to reduction during *T. gondii* infection compared to WT counterparts. However, frequencies of earlier B-cell developmental stages were comparable between genotypes, which both exhibited a significant reduction in CXCL12 concentrations in the BM^{SN} over the course of infection.

Characterization of T-cell, dendritic-cell, NK-cell, and proinflammatory monocyte/macrophage populations in the $LT\beta R^{-/-}$ BM

Next, a detailed analysis of BM immune cell populations, such as T cell, DC, and NK cell (sub)populations was conducted (Table S1 and S2; for gating strategy, see Fig. S5 and S6; absolute cell numbers are given in Fig. S7).

BM T-cell frequencies ($CD3e^+$) were comparable between both genotypes and were not significantly altered during *T. gondii* infection (Fig. 2A Fig. S7a). Interestingly, T-cell subset frequencies differed significantly between both genotypes: double-negative (DN; $CD4^-/CD8^-$) T cells were twofold to threefold lower, while $CD4^+$ and $CD8^+$ T-cell frequencies were higher in $LT\beta R^{/}$ BM compared to WT BM, both prior to and during *T. gondii* infection (Fig. 2b through e). These genotype-dependent differences were also partially observed in the absolute cell numbers for DN T cells and $CD4^+$ T cells but were not statistically significant for $CD8^+$ T cells (Fig. S7b through d).

In addition to B- and T-cells, a striking phenotype was the reduced upregulation of surface major histocompatibility complex class II (MHCII) on proinflammatory ($Ly6C^+$) monocytes/macrophages (defined as $CD3e^-$ $CD19^-$ $NK1.1^-$ $CD11b^+$ $Ly6G^-$ $Ly6C^+$) in the BM of $LT\beta R^{-/-}$ mice (Fig. 2f and g; Fig. S7e). A similar reduction was found in the PB (Fig. S7f) but not in the PerC (Fig. S7g; for gating strategy, see Fig. S8), where MHCII-expressing proinflammatory monocyte/macrophage frequencies were comparable between genotypes. Notably, the overall frequencies of proinflammatory monocytes/macrophages were similar between $LT\beta R^{-/-}$ and WT BM, except on day 9 p.i., where a significant reduction was observed in $LT\beta R^{-/-}$ BM (Fig. 2h). However, this difference was not reflected in the absolute cell numbers (Fig. S7h).

LTβR signaling is also essential for the generation of functional NK cells (13, 109), NKT cells (13, 22, 23), as well as DCs (5, 13, 110). We can confirm these findings in the BM compartment of $LT\beta R^{-/-}$ mice, where basically neither NK (Fig. 2i; Fig. S7i) nor NKT cells (Fig. 2j; Fig. S7j) were detectable before and during *T. gondii* infection, and where pDCs were reduced particularly on day 6 p.i. compared to WT mice (Fig. 2k; Fig. S7k). Notably, BM neutrophil frequencies (Fig. S7l) and numbers (Fig. S7m) did not significantly differ between genotypes. These results show that the absence of LTβR signaling perturbed specific myeloid and lymphoid immune cell populations in the BM.

BM RNA sequencing reveals impaired upregulation of IFNγ- and IFNα-related gene sets concurrent with enriched TNFα signaling and an increased presence of eosinophil-associated transcripts in $LT\beta R^{-/-}$ mice

Sequencing of mRNA (RNASeq) of WT and $LT\beta R^{-/-}$ BM was performed to investigate the BM transcriptome during *T. gondii* infection. Gene set enrichment analysis (GSEA) was employed to compare gene sets between genotypes ($LT\beta R^{-/-}$ vs WT, Fig. 3a; Fig. S9) and across the infection timeline (d6 and d9 p.i. vs. uninfected controls, and d9 vs. d6 p.i., Fig. 3b and c; Fig. S10).

In the genotype comparison (Fig. 3a), the gene sets "Interferon gamma response" and "Interferon alpha response" were significantly enriched in the BM of all WT cohorts compared to $LT\beta R^{-/-}$ counterparts, particularly in uninfected controls and on day 6 p.i. By contrast, the "TNFα signaling via NF-κB" gene set was significantly enriched in $LT\beta R^{-/-}$ BM at all time points examined. Other inflammation-related gene sets, such as "Inflammatory response" and "Reactive oxygen species," were enriched in WT BM or showed no significant difference between genotypes.

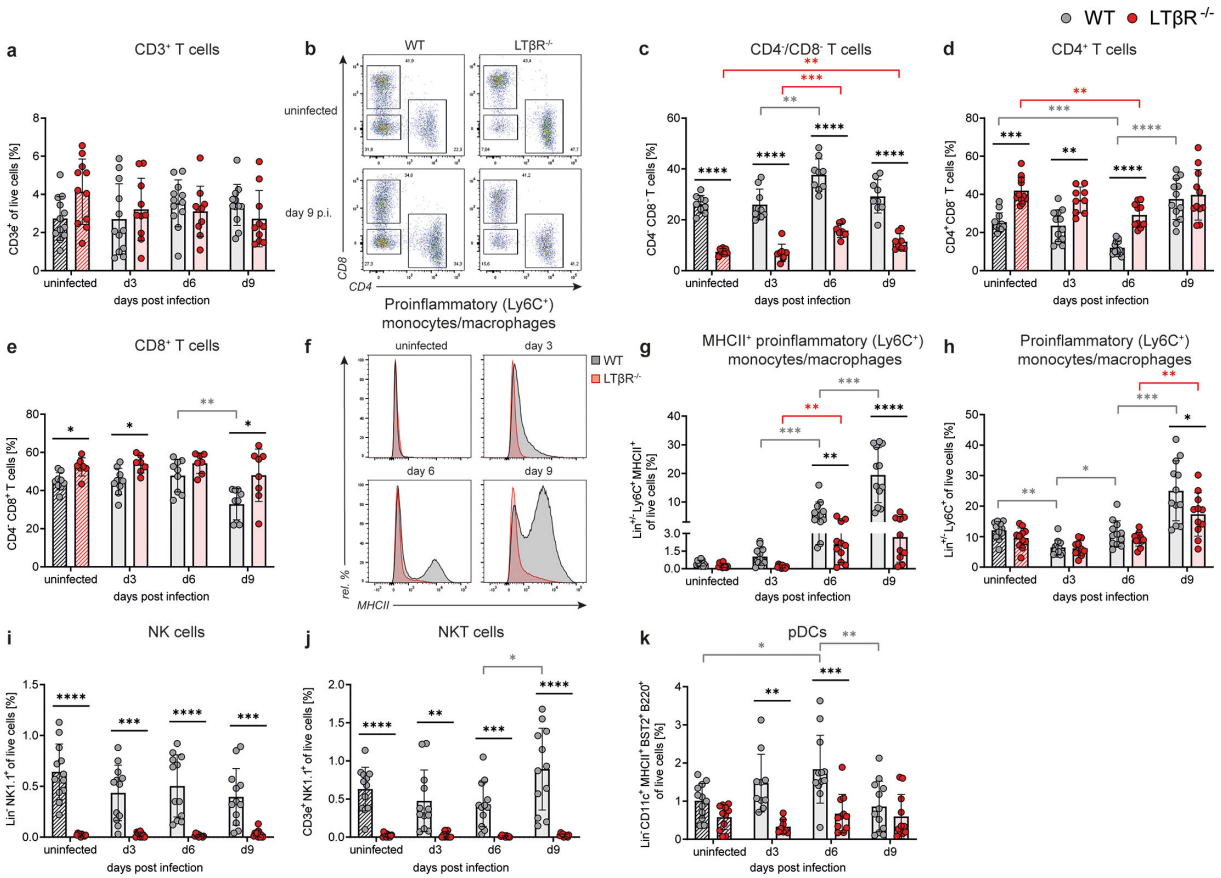

FIG 2 Altered T cells, proinflammatory monocytes/macrophages, NK cells, NKT cells, and pDCs in the BM of *T. gondii*-infected LTβR$^{-/-}$ mice. Using surface marker staining and flow cytometry, the following immune cell populations (gating strategies: Fig. S5 and S6) in the BM of WT and LTβR$^{-/-}$ mice were identified and quantified as percentages of live cells, unless otherwise specified: (a) T cells (CD3e$^+$) (b–e) (b) shows a set of representative images of the gating of (c) double-negative (CD4$^-$ CD8$^-$), (d) CD4$^+$, and (e) CD8$^+$ T cells, all shown as % of CD3e$^+$ T cells. WT: $n \geq 9$/group and LTβR$^{-/-}$: $n \geq 7$/group. (f) Representative histograms of MHCII expression (%) on proinflammatory monocytes/macrophages. Each curve is scaled to 100%. (g) MHCII-positive proinflammatory monocytes/macrophages (CD19$^-$ CD3e$^-$ NK1.1$^-$ CD11b$^+$ Ly6G$^-$ Ly6C$^+$ MHCII$^+$). (h) Proinflammatory monocytes/macrophages (CD19$^-$ CD3e$^-$ NK1.1$^-$ CD11b$^+$ Ly6G$^-$ Ly6C$^+$). (i) NK cells (CD19$^-$ CD3e$^-$ NK1.1$^+$). (j) NKT cells (CD3e$^+$ NK1.1$^+$). (k) Plasmacytoid DCs (pDCs; CD19$^-$ CD3e$^-$ NK1.1$^-$ CD11c$^+$ CD11b$^-$ MHCII$^+$ B220$^+$ BST-2$^+$). All data shown represent at least four independent experiments; symbols represent individual animals and columns represent mean values ± SD. *P < 0.05; **P < 0.01; ***P < 0.001; ****P < 0.0001.

When comparing each infected genotype to its respective uninfected control, both WT (Fig. 3b) and LTβR$^{-/-}$ (Fig. 3c) BM exhibited proinflammatory gene set enrichment, particularly "Interferon gamma response" and "Interferon alpha response," on days 6 and 9 p.i. Notably, these gene sets were less enriched in WT BM on day 9 p.i. compared to day 6 p.i. (Fig. 3b), whereas LTβR$^{-/-}$ BM showed continued enrichment from day 6 to day 9 p.i. (Fig. 3c). The "TNFα signaling via NF-κB," "Inflammatory response," and "Reactive oxygen species" gene sets were enriched in the BM of both genotypes during *T. gondii* infection (Fig. 3b and c). A summary of additional GSEA gene sets is provided in Fig. S9d.

Thus, compared to WT BM, the LTβR$^{-/-}$ BM exhibited reduced enrichment of the critical "Interferon gamma response" and "Interferon alpha response" gene sets but showed greater enrichment of the "TNFα signaling via NF-κB" pathway. Overall, both genotypes displayed increased expression of IFN-related gene sets over the course of *T. gondii* infection, with expression peaking in WT BM on day 6 p.i. but continuing to increase until day 9 p.i. in LTβR$^{-/-}$ BM.

We also identified the top differential transcripts between WT and LTβR$^{-/-}$ BM on days 6 and 9 p.i. Notably, LTβR$^{-/-}$ BM displayed elevated expression of immunoglobulin genes (*Igkc*, *Ighm*, *Iglc2*, and *Ighd*) and specific migration/adhesion genes (*Ccl6*, *Ccl9*, and *Fn1*),

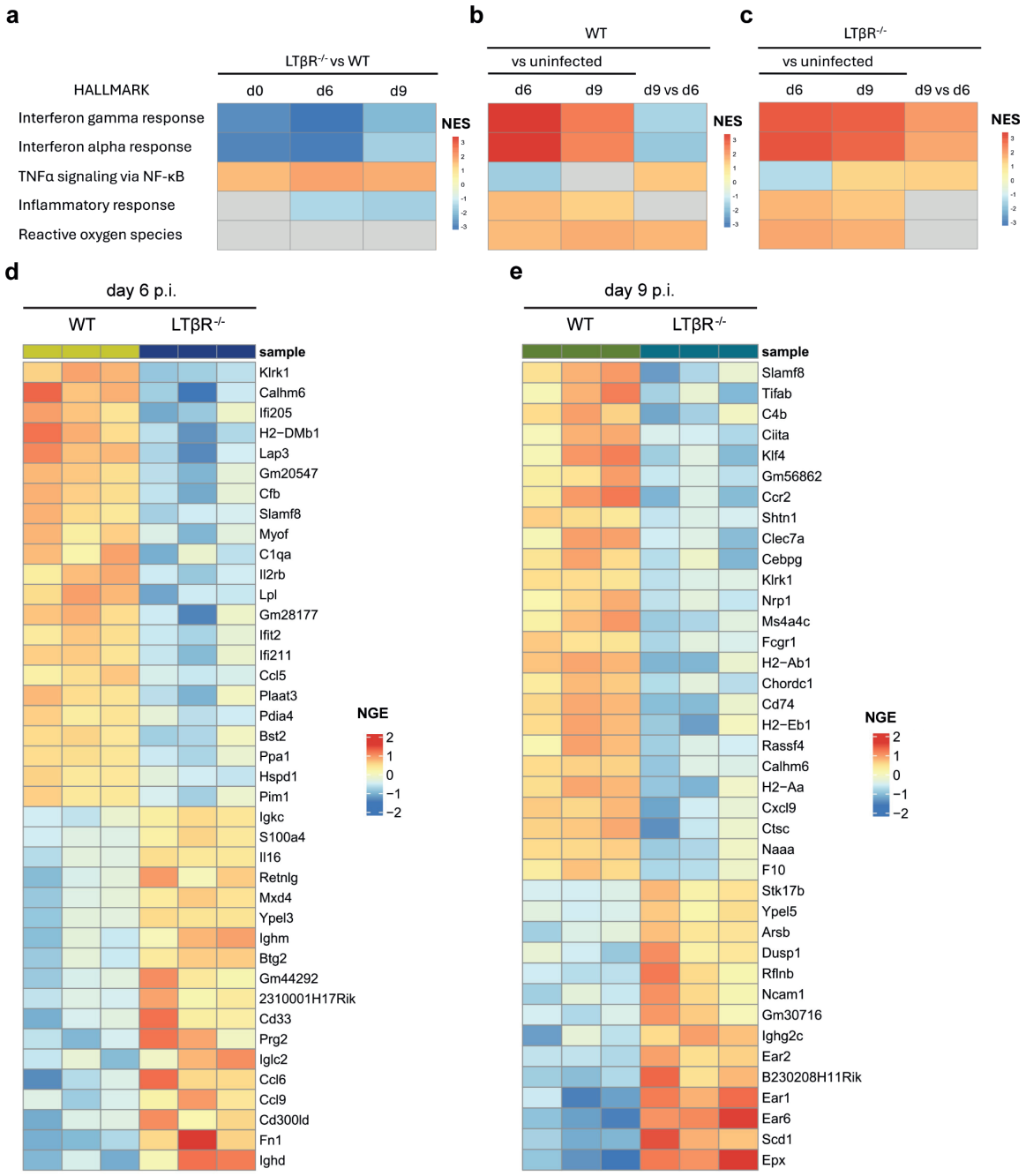

FIG 3 LTβR$^{-/-}$ BM shows less enrichment of interferon-related gene sets compared to WT BM, but more eosinophil-related gene expression on day 9 p.i. (a–c) Summarized results of the gene set enrichment analysis (GSEA) of mRNA sequencing data from BM samples of uninfected and *T. gondii*-infected WT (n = 3/group) and LTβR$^{-/-}$ mice (n = 3, except for LTβR$^{-/-}$ uninfected: n = 2). Normalized enrichment scores (NES) of selected GSEA hallmark gene sets (see Fig. S9a through d and S10 for complete GSEA data) are represented as colors in a heat map. A positive NES value indicates gene set enrichment in the experimental condition, a negative NES value indicates gene set enrichment in the control condition, and a gray-colored tile describes non-significance (adjusted P-value > 0.01). The (a) left panel summarizes genotype comparisons (LTβR$^{-/-}$ vs. WT), displaying enrichment in LTβR$^{-/-}$ compared to WT controls. The (b) middle panel summarizes intra-WT comparisons: d6 and 9 p.i. vs. uninfected controls, displaying enrichment in infected animals; and d9 vs. d6, displaying enrichment on day 9 p.i. compared to day 6 p.i. Similarly, the (c) right panel summarizes intra-LTβR$^{-/-}$ comparisons: d6 and 9 p.i. vs. uninfected controls, displaying enrichment in infected animals; and d9 vs. d6, displaying enrichment on day 9 p.i. compared to day 6 p.i. (d and e) Heat map of the top 40 differentially expressed genes (based on the adjusted P-values) in WT and LTβR$^{-/-}$ BM on (d) day 6 p.i and (e) day 9 p.i., sorted by upregulation and downregulation. NGE = normalized gene expression.

but lower expression of IFNγ-inducible genes (*Ifi205*, *Ifit2*, *Ifi211,* and *Bst2*) compared to WT BM on day 6 p.i. (Fig. 3d). On day 9 p.i., transcripts of several members of the eosinophil-associated ribonuclease A family (*Ear1*, *Ear2,* and *Ear6*) and *Epx* (eosinophil peroxidase) were significantly increased in LTβR$^{-/-}$ BM (Fig. 3e), whereas expression of genes associated with MHCII and antigen presentation (*Ciita*, *H2-Ab1*, *H2-Aa*, *H2-Eb1,* and *CD74*), immune cell function (*Klrk1* and *Fcgr1*), and migration (*Ccr2* and *Cxcl9*) was decreased compared to WT BM (Fig. 3e). *Slamf8* transcripts, which are expressed by a variety of activated myeloid cells, including IFNγ-activated monocytes and macrophages (111), were reduced on both days in LTβR$^{-/-}$ BM. Interestingly, only a small number of *T. gondii*-derived transcripts were detected, with the majority being identified in LTβR$^{-/-}$ BM on day 9 p.i., primarily encoding GRA (*T. gondii* dense granule organelle) proteins (Fig. S9e).

Leukocyte counts, *T. gondii* burden, and dead cell frequencies are elevated in the PerC of LTβR$^{-/-}$ mice

The number of *T. gondii* tachyzoites in the PerC as the primary site of infection was significantly increased and 10-fold higher in LTβR$^{-/-}$ compared to WT mice on day 9 p.i. (Fig. 4a). Both genotypes exhibited elevated peritoneal leukocyte counts compared to their respective uninfected controls. However, peritoneal leukocyte numbers were significantly higher in LTβR$^{-/-}$ mice compared to WT mice, both before infection and on days 3 and 9 p.i. (Fig. 4b). In addition, most but not all mice of both genotypes developed ascites by day 9 p.i. (data not shown). The frequency of dead cells within the total leukocyte population was found to be comparable between genotypes in uninfected controls and early during infection, but significantly higher in LTβR$^{-/-}$ mice on days 6 and 9 p.i. (Fig. 4c). Due to the higher leukocyte counts in the LTβR$^{-/-}$ PerC, the absolute number of dead cells was increased at all analyzed time points (Fig. S11a). In summary, LTβR$^{-/-}$ mice exhibited increased leukocyte counts coupled with higher parasite burden and elevated dead cells.

Frequencies of B-2 and B-1b, but not B-1a cells, were increased in the PerC of LTβR$^{-/-}$ mice

Similar to the BM phenotype, B-cell frequencies as well as absolute numbers in the PerC were significantly increased in LTβR$^{-/-}$ mice before and during *T. gondii* infection (Fig. 4d; Fig. S11b). The frequency of peritoneal B cells was significantly reduced on day 9 p.i. in WT (−95.8% on day 9 p.i. compared to uninfected) and, to a slightly lesser extent, in LTβR$^{-/-}$ mice (−90.6% on day 9 p.i. compared to uninfected).

In addition to conventional B-2 cells (CD19^{+} B220^{high}), the PerC was enriched with B-1 cells (CD19^{+} B220^{low}), a special B-cell subset with distinct origins, phenotypes, and functions (114, 115). Both B-1 and B-2 frequencies were increased in uninfected LTβR$^{-/-}$ mice (Fig. 4e through g, see Fig. S11c and d for absolute cell numbers). During infection, B-2 cell populations initially remained stable but then dropped between days 6 and 9 p.i. (Fig. 4f). By contrast, B-1 cell frequencies already dropped significantly by day 3 p.i. and then again between days 6 and 9 p.i. (Fig. 4g). Serum concentrations of CXCL13, a chemokine essential for B-1 cell functionality and mobility (116, 117), increased during the course of infection and were markedly elevated on day 6 and especially day 9 p.i., but remained comparable between WT and LTβR$^{-/-}$ mice (Fig. 4h). Similar kinetics were observed in the BM^{SN} (Fig. S11e).

B-1 cells can be further classified into B-1a and B-1b cells based on their CD5 surface marker expression (Fig. S11f). The PerC B-1a to B-1b ratio of LTβR$^{-/-}$ mice was roughly 1:1 (with slightly higher B-1b frequencies), which shifted in favor of the B-1a population over the course of infection (Fig. 4i). By contrast, WT B-1 cells mainly consisted of B-1a cells (72.0% ± 5.8 %), which slightly decreased over the course of infection. Importantly, the shift in LTβR$^{-/-}$ B-1a to B-1b frequencies was not caused by a reduction in B-1a but rather an increase in B-1b frequencies, as determined by B-1a and B-1b live cell frequencies (Fig. 4j and k). This was also confirmed through a direct B-1a (CD19^{+} CD5^{+}) gating without prior B-1 gating (Fig. S11g and h). Thus, B-1a cell frequencies were comparable, and B-1b

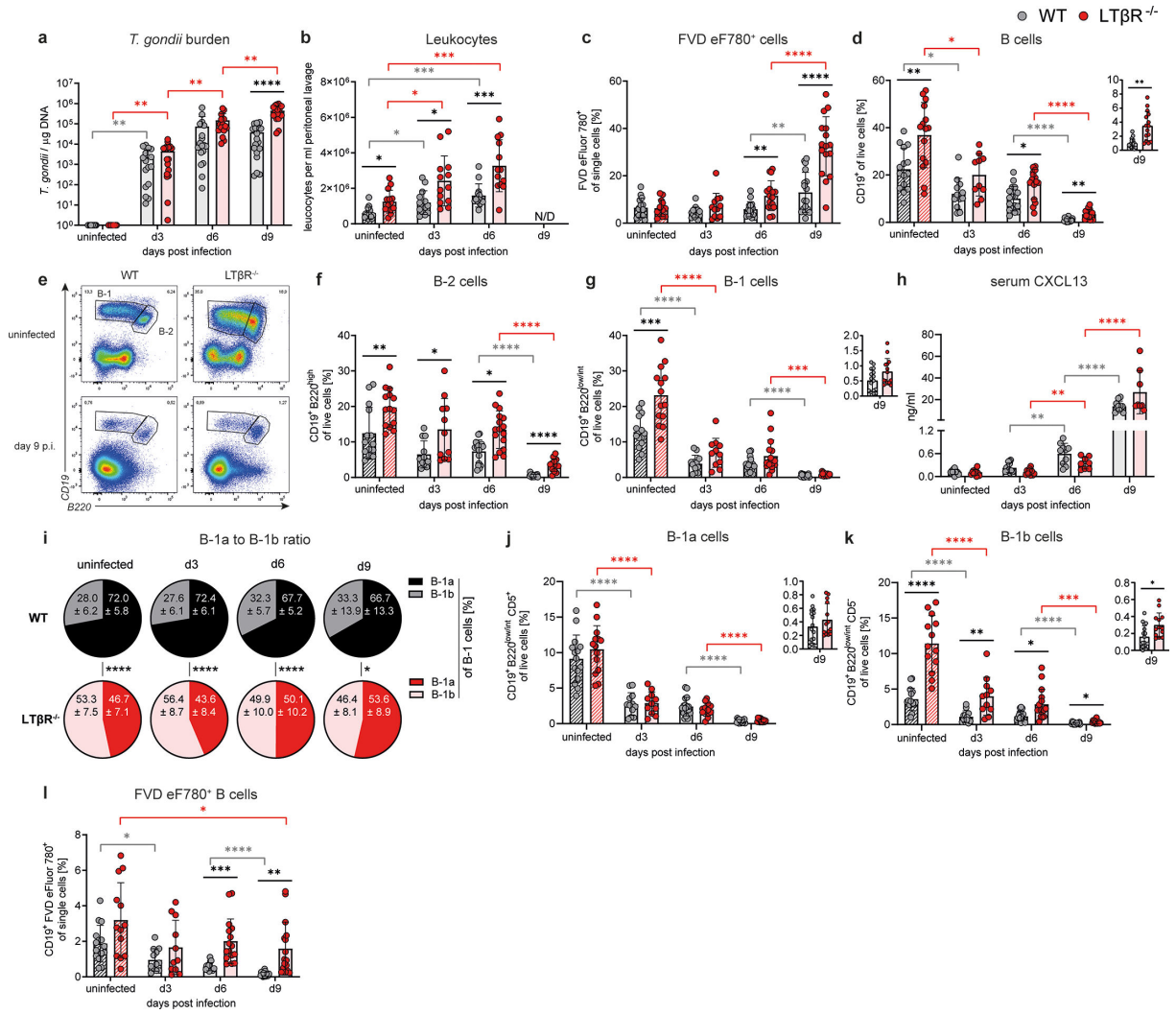

FIG 4 Altered B-cell subpopulations in the PerC of *T. gondii*-infected WT and LTβR$^{-/-}$ mice. (a) DNA was isolated from cells obtained by peritoneal lavage of uninfected and *T. gondii*-infected WT ($n \geq 14$/group) and LTβR$^{-/-}$ ($n \geq 12$/group) mice and used to assess parasite burden via quantitative real-time PCR of the *T. gondii* B-1 gene (*TgB1*). A standard curve generated from a defined number of ME49 tachyzoites (2,914 ± 214 /µL) was used to calculate parasite loads. (b) Counted peritoneal leukocytes per mL lavage from uninfected and infected WT and LTβR$^{-/-}$ mice (both $n \geq 13$/group). Peritoneal lavage was performed by injection of 5 mL ice-cold PBS, followed by a gentle massage and subsequent recovery of fluid. No reliable cell count can be reported for day 9 p.i. due to large amounts of cell debris and clumped cells. Exclusion of all non-single-cell events during flow cytometry enabled the analysis of the remaining single cells. Using surface marker staining and flow cytometry, the following immune cell populations (gating strategy: Fig. S8) in the PerC of WT ($n \geq 12$/group) and LTβR$^{-/-}$ ($n \geq 11$/group) mice were identified and quantified as percentages of live cells, unless otherwise specified: (c) Dead leukocytes (FVD eFluor780$^+$), % of single cells. (d) B cells (CD19$^+$). (e–g) B-1 (CD19$^+$ B220$^{low/int}$) and B-2 (CD19$^+$ B220^{high}) cells. (e) A set of representative images. Please note that the large CD19$^-$ B220$^+$ cell population in uninfected mice was found to be large CD11b$^+$ Ly6G$^-$ Ly6C$^-$ cells, which represent autofluorescent large tissue-resident macrophages that disappear after infection (112, 113). (h) CXCL13 measured in the serum of uninfected and infected WT ($n \geq 10$) and LTβR$^{-/-}$ ($n \geq 8$) *via* bead-based immunoassay (LegendPlex, BioLegend, USA). (i) Ratios of B-1a (CD19$^+$ B220$^{low/int}$ CD5$^+$) to B-1b (CD19$^+$ B220$^{low/int}$ CD5$^-$) cells, % of B-1 cells. (j and k) Frequencies of B-1a (CD19$^+$ B220$^{low/int}$ CD5$^+$) and B-1b (CD19$^+$ B220$^{low/int}$ CD5$^-$) cells. (l) Dead B cells (CD19$^+$ FVD eFluor780$^+$), % of single cells. All data shown represent at least three independent experiments; symbols represent individual animals and columns represent mean values ± SD. *$P < 0.05$; **$P < 0.01$; ***$P < 0.001$; ****$P < 0.0001$.

cell frequencies were increased in LTβR$^{-/-}$ compared to WT mice. Both B-1 subpopulations showed a biphasic decrease (from uninfected to day 3 and from day 6 to 9 p.i.). While B-1a cell frequencies were comparable between genotypes, the absolute numbers of B-1a cells were higher in the LTβR$^{-/-}$ PerC due to the increased total leukocyte count (Fig. 4b; Fig. S11i and j). Dead peritoneal B cells (FVD eF780$^+$) were significantly higher in LTβR$^{-/-}$ mice, particularly on days 6 and 9 p.i. (Fig. 4l; Fig. S11k).

In summary, in LTβR$^{-/-}$ mice, the increased B-2 cell phenotype includes both the BM and PerC compartments. In uninfected LTβR$^{-/-}$ mice, B-1b frequencies were increased and shifted the B-1a to B-1b ratio, whereas B-1a frequencies remained comparable to the WT PerC. After *T. gondii* infection, both genotypes displayed a marked reduction in B-1 cell frequencies on day 3 p.i., which was absent for B-2 cells.

LTβR$^{-/-}$ PerC immune cell composition is dominated by neutrophils instead of T cells in late acute *T. gondii* infection

Neutrophils were almost absent in the PerC of uninfected controls but increased significantly in both genotypes during *T. gondii* infection (Fig. 5a and b; Fig. S12a). By day 9 p.i., they dominated the peritoneal immune cell composition in LTβR$^{-/-}$ mice (48.4 ± 14.4 %), whereas (CD4$^+$) T cells were the major population in WT mice (42.4 ± 15.6 % pan-T cells, Fig. 5c and d). Peritoneal T-cell subset frequencies were more similar between genotypes than those in the BM (Fig. 3a through e) but still showed genotype-specific differences in DN T cells (Fig. 5e), CD4$^+$ T cells (Fig. 5f), and CD8$^+$ T cells (Fig. 5g). Notably, uninfected LTβR$^{-/-}$ PerCs had increased CD4$^+$ and reduced CD8$^+$ T-cell frequencies compared to WT mice, indicating altered peritoneal T-cell composition even before infection. By contrast, by day 9 p.i., LTβR$^{-/-}$ PerCs displayed reduced CD4$^+$ and higher CD8$^+$ T-cell frequencies compared to WT. Regarding absolute cell numbers, DN T cells differed significantly between genotypes in uninfected mice and on day 6 p.i., whereas CD4$^+$ T cells and CD8$^+$ T-cell numbers showed no statistically significant differences (Fig. S12b through e).

LTβR$^{-/-}$ mice display increased inflammatory infiltrates in the lung and liver

A necropsy of lung, liver, brain, kidney, spleen, and BM, followed by histological analysis, was performed to further investigate the impact of LTβR deficiency during *T. gondii* infection. LTβR$^{-/-}$ mice are known to exhibit abnormal lymphocytic infiltrations in the lung

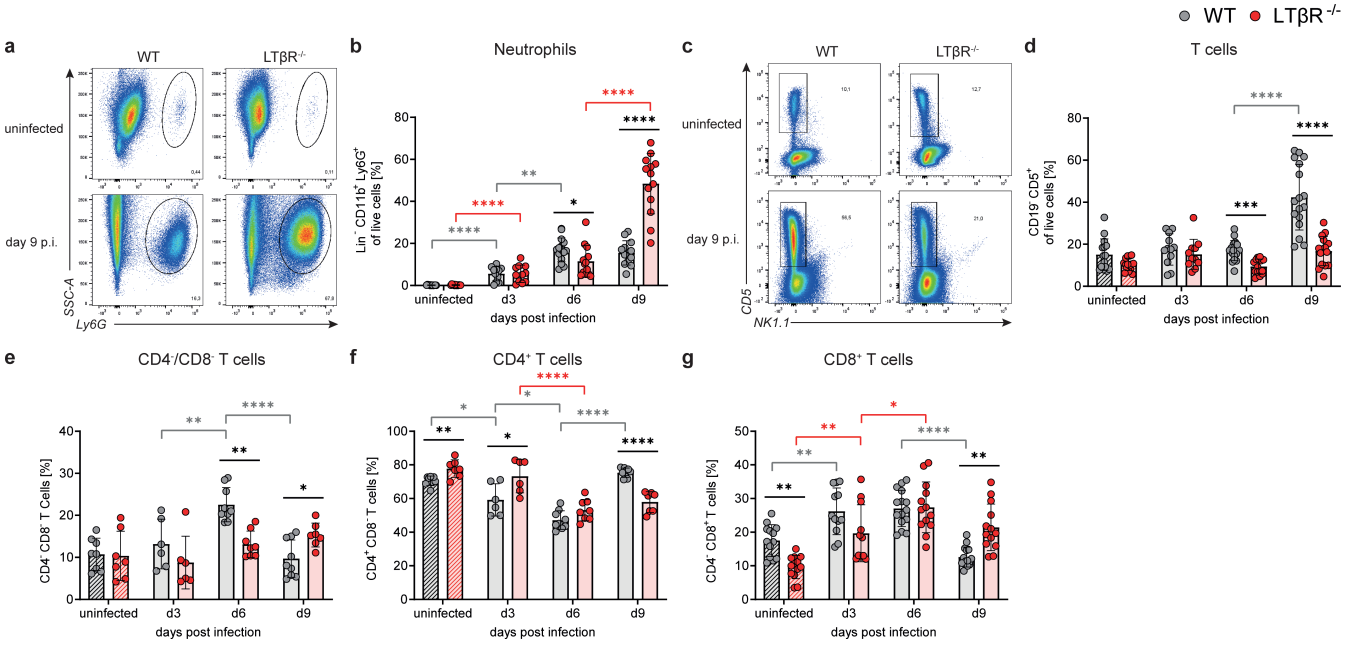

FIG 5 Neutrophils, instead of T cells, dominate the PerC immune cell composition of LTβR$^{-/-}$ mice on day 9 p.i. during *T. gondii* infection**.** Using surface marker staining and flow cytometry, the following immune cell populations (gating strategy: Fig. S8) in the PerC of WT ($n \geq 12$/group) and LTβR$^{-/-}$ ($n \geq 11$/group) mice were identified and quantified as percentages of live cells, unless otherwise specified: (a and b) neutrophils (CD19$^-$ CD5$^-$ NK1.1$^-$ CD11b$^+$ Ly6G$^+$). (a) A set of representative images. (c and d) T cells (CD19$^-$ CD5$^+$). (c) A set of representative images. (e–g) Double-negative (CD4$^-$ CD8$^-$), CD4$^+$ and CD8$^+$ T cells, % of T cells. WT: $n \geq 6$/group, LTβR$^{-/-}$: $n \geq 6$/group. All data shown represent at least three independent experiments; symbols represent individual animals and columns represent mean values ± SD. *$P < 0.05$; **$P < 0.01$; ***$P < 0.001$; ****$P < 0.0001$.

even in the absence of infection (11, 13, 118), a finding also evident in our histological analysis (Fig. 6). *T. gondii* infection increased lung infiltration compared to uninfected controls, with LTβR$^{-/-}$ mice exhibiting more pronounced inflammatory infiltrates than WT mice, consistent with their baseline phenotype. After infection, WT animals showed minimal pulmonary pathology, characterized by mild, scattered monocytic infiltration on day 9 p.i., whereas LTβR$^{-/-}$ lungs displayed increased perivascular and pleural mixed inflammatory infiltrates on days 6 and 9 p.i. (Fig. 6).

T. gondii infection also led to more pronounced inflammatory infiltrates in the liver of LTβR$^{-/-}$ compared to WT mice, mirroring the lung phenotype. The liver of WT mice displayed multifocal inflammatory foci occasionally associated with necrotic cells, as well as marked capsular and minimal perivascular/periportal inflammation (Fig. 7). On day 6 p.i., these inflammatory/necrotic foci were few, scattered, and dominated by neutrophils and cellular debris (acute necrosis); on day 9 p.i., foci were more numerous, with often macrophages predominating (subacute necrosis). By contrast, the livers of LTβR$^{-/-}$ mice displayed more extensive inflammation, with predominantly (sub)capsular, perivascular, and mixed mononuclear infiltrates, and randomly scattered areas of multiple hepatocellular necrosis and neutrophilic inflammation. Large numbers of monocytes were usually visible within the lumen of large-caliber vessels (monocytic leukocytosis). On day 6 p.i., inflammatory foci were few and <50% of vessels were affected. On day 9 p.i., most vessels had perivascular mixed mononuclear inflammation, parenchymal foci were increased in number, and macrophages predominated (subacute necrosis).

Neither the brain nor BM displayed genotype-specific differences in the histological analysis (data not shown). WT and LTβR$^{-/-}$ BM had mild to moderately increased granulopoiesis on days 6 and 9 p.i., as evident by increased ratios of myeloid to erythroid

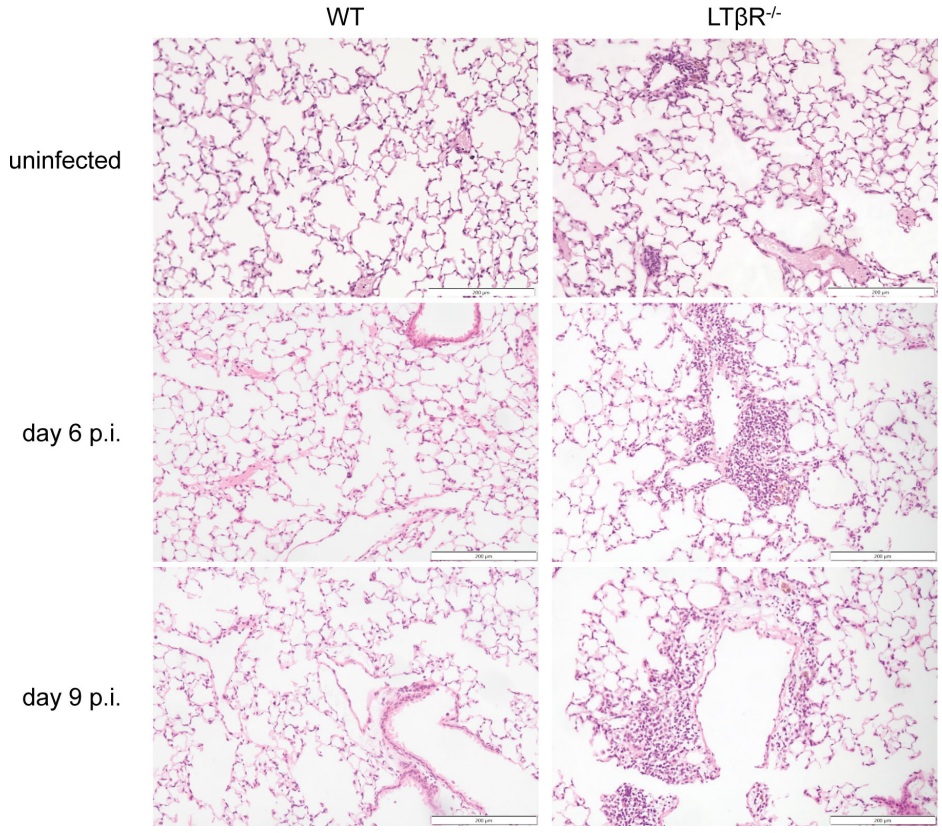

FIG 6 LTβR$^{-/-}$ mice exhibit more inflammatory infiltrations in the lung during *T. gondii* infection. Representative images of H&E-stained lungs from uninfected and *T. gondii*-infected WT and LTβR$^{-/-}$ mice. $n = 3$ except for LTβR$^{-/-}$ uninfected ($n = 1$). Scale bar: 200 µm.

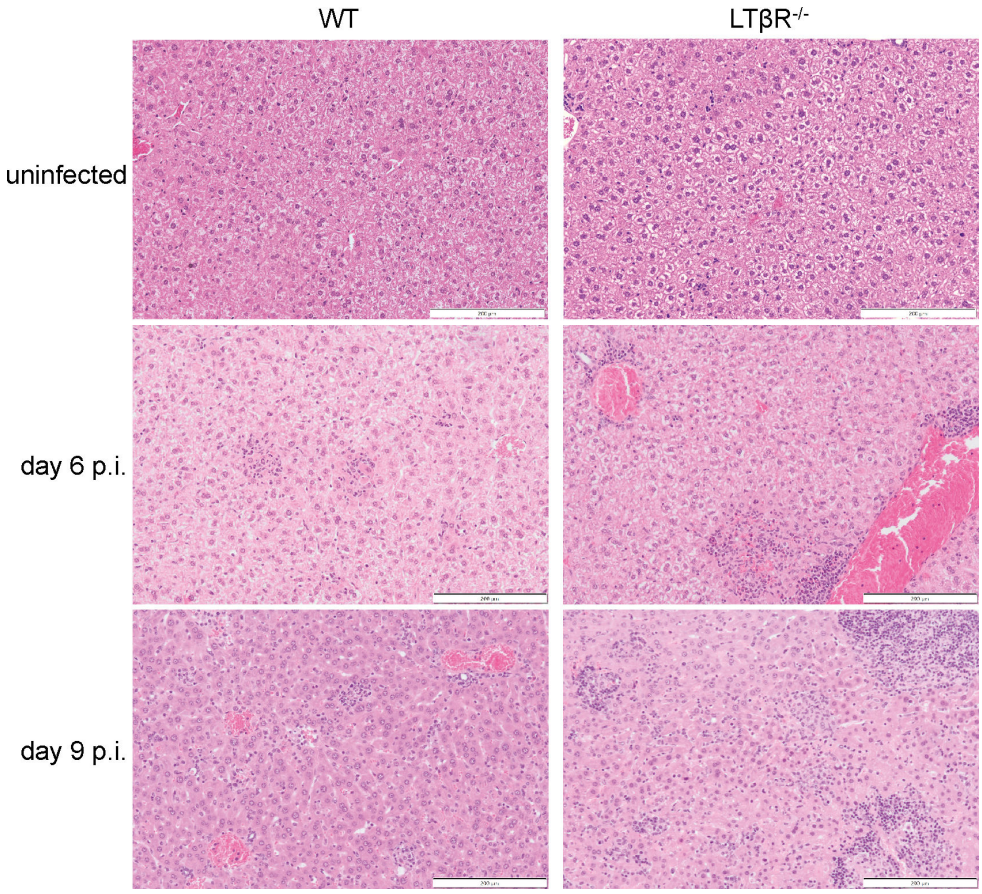

FIG 7 LTβR$^{-/-}$ mice exhibit more inflammatory infiltrations in the liver during *T. gondii* infection. Representative images of H&E-stained livers from uninfected and *T. gondii*-infected WT and LTβR$^{-/-}$ mice. $n = 3$ except for LTβR$^{-/-}$ uninfected ($n = 1$). Scale bar: 200 µm.

cells (data not shown). The kidneys displayed mild to moderate capsular inflammatory infiltrations, but no genotype-specific differences (Fig. S13).

DISCUSSION

B cells play a crucial role in both protective and, counterintuitively, sometimes in disease-aggravating responses during protozoan parasite infections (83, 87, 100, 101). LTβR$^{-/-}$ mice, which exhibit high susceptibility to *T. gondii* infection, show a compromised ability to generate parasite-specific IgM and IgG responses (25). In this study, we investigated the different immune cell compartments (with a focus on B cells) in homeostasis and the impact of absent LTβR signaling on B-cell populations in the BM and PerC of LTβR$^{-/-}$ mice during *T. gondii* infection.

In adult mice, B-2 cell development initially occurs in the BM, with most immature B cells then migrating to the spleen to complete their development, while some mature within the BM itself (91, 119, 120). Uninfected LTβR$^{-/-}$ mice exhibited an increased number of B cells in the BM compared to WT mice, with mature B cells (IgD^{high}) being identified as the predominant subset. In the BM, these recirculating mature B cells normally reside in extravascular perisinusoidal niches alongside T cells, monocytes, and BMDCs, where they receive survival signals such as B cell-activating factor (BAFF) and macrophage migration inhibitory factor (MIF), and contribute to immune responses against blood-borne pathogens (120–122). A disruption of this niche, particularly alterations in the expression of membrane-bound and secreted molecules involved in chemotaxis and adhesion, may contribute to the increased accumulation of mature B cells in the LTβR$^{-/-}$

BM. While LTβR signaling is known to regulate immune cell migration by controlling adhesion molecule and chemokine expression in SLOs (15, 123–125) and the thymus (26, 126, 127), its role in shaping the BM microenvironment and guiding B-cell chemotaxis remains poorly understood. LTβR signaling, particularly via $LT\alpha_1\beta_2$ engagement, is essential for T-cell progenitor homing to the thymus (128–130), the organization of its medullary architecture (26, 27, 131), and the egress of mature T cells, which relies on a specific LTβR-dependent endothelial subset known as portal endothelial cells (27, 130, 132). Given this role in thymocyte egress, it is conceivable that LTβR signaling similarly facilitates egress of mature B cell from the BM.

While these results warrant further investigation of the BM microenvironment, the increase in B cell frequency/number is not restricted to the BM but is also present in the spleen (25) and, as we have shown here, in the PerC of uninfected $LT\beta R^{-/-}$ mice. As with BM B cells, alterations in the local microenvironment and/or chemotaxis may contribute to this phenotype. In addition, the absence of SLOs in $LT\beta R^{-/-}$ mice, including LNs and gut-associated lymphatic tissue (GALT) (11), may promote the accumulation of mature B cells in alternative compartments such as the BM and the PerC.

In the PerC of uninfected $LT\beta R^{-/-}$ mice, B-1a cells were a notable exception to the otherwise increased B-cell frequencies compared to WT mice. In our previous study, a host-pathogen network prediction model based on RNASeq data from murine lung tissue following *T. gondii* infection suggested that LTβR deficiency could upregulate the "B-cell receptor signaling pathway" gene set (25). If altered BCR signaling contributes to the observed B-cell phenotype in $LT\beta R^{-/-}$ mice, the relative unresponsiveness of peritoneal B-1 cells (93, 133–135) - particularly B-1a cells (136, 137) - to BCR stimulation, compared to B-2 cells, may explain why B-1a cells remained unaffected despite the overall increase in B-cell frequencies in $LT\beta R^{-/-}$ mice. Notably, although B-1a cell frequencies were comparable to those of WT mice, their absolute numbers were elevated due to an expanded leukocyte compartment in the $LT\beta R^{-/-}$ PerC.

In addition to the B-cell compartment, we also observed changes in the T-cell compartment in the BM of uninfected $LT\beta R^{-/-}$ mice. In contrast to BM B cells, BM T cells ($CD3e^+$) were not substantially increased in $LT\beta R^{-/-}$ mice, despite their shared capability to express LTβR ligands, their overlapping BM niches (122), and their similarly increased presence in PB and tissue infiltrations in $LT\beta R^{-/-}$ mice (11). However, the significant shift in subset frequencies, characterized by a decrease in DN T cells and an increase in $CD4^+$ and $CD8^+$ T cells, indicates that LTβR deficiency does impact the BM T-cell compartment. While DN T cells are enriched in the BM (77), their origin remains rather unclear, with evidence supporting both thymus-dependent and thymus-independent pathways, including differentiation from both $CD4^+$ and $CD8^+$ T cells (78, 138). The absence of LTβR signaling may disrupt DN T-cell development or migration, leading to their reduced frequencies in the BM. Notably, uninfected $LT\beta R^{-/-}$ mice exhibit increased numbers of $CD4^+$ (and $CD8^+$) T cells in the thymus (27, 132), and $CD4^+$ regulatory T cells (T_{regs}) are particularly dependent on $LT\alpha_1\beta_2$-LTβR interactions for efficient transendothelial migration (139, 140). Our data, therefore, clearly show that the absence of LTβR signaling also affects the BM T-cell compartment.

During inflammation, the BM microenvironment is disrupted, with lymphopoiesis suppressed in favor of emergency granulopoiesis to replenish the depleted granulocyte compartment for host defense (141–143). While uninfected $LT\beta R^{-/-}$ mice had significantly higher B-cell numbers and frequencies in the BM compared to WT mice, *T. gondii* infection led to a marked reduction in early-stage B-cell subsets in both genotypes. By contrast, later-stage subsets, particularly mature B cells, were significantly more resistant to inflammation-induced reduction compared to their WT counterparts. Similar reductions in early-stage B cells have been reported during infections with other protozoan parasites, such as *Trypanosoma brucei* (144) and *Plasmodium chabaudi* (145); however, mature BM B cells were not assessed in these studies. The reduction of early-stage B cells has been linked to the chemokine CXCL12, which is essential for B-cell development and regulates their retention in the BM through the very late antigen

4 (VLA-4/integrin $\alpha_4\beta_1$) and vascular cell adhesion protein 1 (VCAM-1) axis (146–150). Proinflammatory cytokines, particularly TNFα and IL-1β, downregulate stromal CXCL12 expression, promoting the egress of lymphocytes, including early-stage B cells, into the blood (107). Notably, while both LTβR$^{-/-}$ and WT mice had reduced CXCL12 concentrations in their BM during infection, we did not detect a significant increase in early-stage B cells in the PB on day 9 p.i. Given their exceptional sensitivity to apoptosis (151) and the advanced stage of early B-cell depletion, it is conceivable that most mobilized early-stage B cells were cleared from the circulation by the time of analysis on day 9 p.i.

During B-cell development, sensitivity to CXCL12-guided chemoattraction gradually declines as CXCR4 expression decreases, allowing later-stage B cells to exit the BM (147, 150). However, unlike circulating B cells, mature BM B cells still respond to sustained CXCL12-induced adhesion, albeit to a lesser extent than earlier B-cell subsets (147). Blocking CXCL12 signaling via CXCR4 depletion in CD19$^+$ BM B cells increases their localization to BM sinusoids rather than the parenchyma and significantly reduces mature B-cell numbers in the BM (149). However, this reduction may, in part, result from disrupted MIF signaling, as MIF is a critical survival factor for mature B cells in the BM (152, 153), acting through CXCR4 (and CXCR2) (154, 155). In addition, B-cell homing to the BM is impaired in mice with reduced CXCL12 expression (107). Collectively, these findings indicate that CXCL12 remains important for mature B-cell retention and localization within the BM, even if their responsiveness to its signals diminishes over time. Therefore, while the CXCL12-dependent reduction of early and mature B cells in WT BM during inflammation aligns with previous findings, mature BM B cells in infected LTβR$^{-/-}$ mice remained unaffected despite CXCL12 reduction, suggesting retention through altered or unknown mechanisms during systemic inflammation. Notably, while our BM transcriptome data revealed genotype-dependent differences in the expression of certain migration- and adhesion-related genes, no substantial differences were observed in the expression of mRNAs of typical LTβR-inducible adhesion molecules, such as *Vcam1*, intercellular adhesion molecule 1 (*Icam1*), *Sele* (E-selectin), and mucosal vascular addressin cell adhesion molecule 1 (*Madcam1*) (10, 20, 125, 127, 156), either between genotypes or during *T. gondii* infection. The regulation of these adhesion molecules in the BM in the absence of LTβR signaling requires further investigation.

Furthermore, BMPCs (TACI$^+$ CD138$^+$) were comparable between genotypes or even increased in LTβR$^{-/-}$ mice on day 9 p.i., despite the absence of LNs and GALT and defective splenic GC formation in these mice (11, 13, 17). Alternative PC differentiation in the BM, independent of GC maturation or T-cell help (120, 157, 158), and/or B-1 cell-derived BMPCs (CD138$^+$), a key source of natural IgM (97, 115), could account for the observed IgM$^+$ BMPCs in LTβR$^{-/-}$ mice. The marked reduction of IgA$^+$ BMPCs aligns with reports of impaired IgA production in LTβR$^{-/-}$ mice (13, 123, 159). IgA production primarily occurs in the GALT, including PPs (160), mesenteric lymph nodes (MLNs) (161), and the lamina propria (LP) (162); however, PPs and MLNs are absent in LTβR$^{-/-}$ mice (11), and recruitment of B cells into the LP is dependent on LTβR expression of LP stromal cells (123). Overall, LTβR signaling appears crucial for IgA$^+$ PC generation, prior to and after pathogen infection.

T. gondii infection also affected the PerC B-cell compartment, which contains both B-1 cells and conventional B-2 cells. While the frequencies of both subsets were markedly reduced on day 9 p.i. in both genotypes, an earlier reduction of B-1 cells was observed on day 3 p.i., whereas B-2 cells remained unchanged at this point. Peritoneal B-1 cell reduction has been reported following i.p. infections, with kinetics ranging from as early as 3 hours (after *Escherichia coli* injection, associated with increased B-1 cell egress [117]) to up to 15 days (after *Trypanosoma cruzi* infection, linked to B-1 cell differentiation into peritoneal PCs rather than increased apoptosis [163]). Given the early onset of B-1 cell reduction, we hypothesize that B-1 cell egress with kinetics specific to an intraperitoneal *T. gondii* infection accounts for this decline. CXCL13, which mediates peritoneal B-1 cell migration (116, 117), showed no genotype-specific differences in the serum or BM^{SN}. Notably, while CXCL13 production in SLOs is LT$\alpha_1\beta_2$-dependent and primarily derived

from follicular stromal cells and FDCs (13, 15, 124, 164–166), macrophages serve as major producers of CXCL13 in the PerC, independent of $LT\alpha_1\beta_2$-LTβR signaling (116, 117, 167, 168). While we hypothesize functional CXCL13-induced B-1 cell egress from the PerC in $LT\beta R^{-/-}$ mice, their fate remains unknown due to the severe alteration or absence of SLOs in these mice.

In addition, the $LT\beta R^{-/-}$ PerC contained higher leukocyte numbers even before *T. gondii* infection, suggesting an elevated basal immune activation status, consistent with previous reports of tissue infiltration by $CD4^+$ T cells and B cells, as well as autoantibody production in $LT\beta R^{-/-}$ mice under steady-state conditions (11, 13, 25, 118). During *T. gondii* infection, $LT\beta R^{-/-}$ PerC leukocyte numbers remained significantly elevated compared to the WT PerC. Necropsy revealed moderate to marked perivascular inflammatory infiltrates in the lungs and livers of $LT\beta R^{-/-}$ mice, which were less pronounced in WT animals. These results indicate altered lymphocyte migration, as discussed earlier, or differences in infection dynamics and immune responses between genotypes.

Furthermore, on day 9 p.i., the $LT\beta R^{-/-}$ PerC immune cell composition was dominated by neutrophils instead of T cells and showed increased cell death, both in contrast to WT PerC. LTβR signaling has been shown to regulate neutrophil metabolism and prevent excessive inflammation (3). While we did not assess their functionality, the accumulation of neutrophils in the $LT\beta R^{-/-}$ PerC, along with increased cell death, may indicate exacerbated peritoneal inflammation and potential immune pathology in these mice.

Overall, the BM transcriptome data indicate that although the immune response, particularly IFN-related genes, was upregulated during *T. gondii* infection in $LT\beta R^{-/-}$ BM, it remained markedly diminished compared to the WT BM. This includes significantly lower expression of multiple genes associated with MHCII and antigen presentation, which aligns with our finding of reduced MHCII surface expression on proinflammatory ($Ly6C^+$) monocytes/macrophages in $LT\beta R^{-/-}$ BM. During *T. gondii* infection, $Ly6C^+$ monocytes and their precursors are primed with IFNγ from activated NK cells before BM egress, promoting MHCII upregulation (169, 170). Given the near absence of NK cells in $LT\beta R^{-/-}$ mice (13, 24), including in the BM (as shown in this study), the impaired monocyte activation likely reflects a disrupted IFNγ-driven priming process. This also aligns with previous reports of a significantly delayed systemic IFNγ response in $LT\beta R^{-/-}$ compared to WT mice (25, 29). Notably, while IFN-related gene set enrichment persisted in $LT\beta R^{-/-}$ BM throughout the infection, its decline from day 6 to day 9 p.i. in WT BM suggests immune downregulation, likely reflecting emerging parasite control and the need to prevent excessive immunopathology.

In addition, the $LT\beta R^{-/-}$ BM showed a consistent enrichment of the "TNFα signaling via NF-κB" gene set across all investigated time points. Since this enrichment was already present in uninfected mice, it is unlikely to be driven by *T. gondii* infection but may instead represent a compensatory mechanism attempting to counterbalance the absence of LTβR signaling (171). Given that the LTβR and TNF receptors (TNFR1/TNFRp55 and TNFR2/TNFRp75) share downstream signaling components of the classical NF-κB pathway (172–174), activation of these could explain the observed enrichment. However, as these findings are based on bulk RNA sequencing, it remains unclear whether this enrichment occurs broadly across cell populations or is restricted to specific TNF-responsive cells, and the underlying mechanism(s) require further investigation.

In conclusion, our study identifies distinct and novel alterations in immune cell (sub)populations in $LT\beta R^{-/-}$ mice before and during *T. gondii* infection. This includes elevated frequencies of mature B cells in the BM and PerC, unaltered B-1a cell frequencies in the PerC, and reduced DN T cell frequencies in the BM. While LTβR signaling was previously known to influence T-cell migration and development in the thymus, the results from this study strongly suggest that LTβR signaling also plays an important role in the homeostasis and/or migration of mature B cells in the BM and PerC. In addition, our study provides valuable insights into the BM transcriptome in the absence of LTβR expression during protozoan parasite infection, thereby contributing to a deeper

understanding of the complex and multifaceted roles of LTβR signaling in immune responses.

MATERIALS AND METHODS

Mice

LTβR$^{-/-}$ mice were described previously (11) and back-crossed to a C57BL6/N background for at least 10 generations. Wild-type (WT) littermates were used as controls. Mice were housed in the animal facility of the Heinrich Heine University Düsseldorf under specific-pathogen-free (SPF) conditions and were 8 to 16 weeks old at the time of infection. CD1 mice from Charles River Breeding Laboratories were used to maintain and propagate ME49 *Toxoplasma gondii* for infection experiments. All animal experiments were conducted in strict accordance with the German Animal Welfare Act. The protocols were approved by the local authorities (Permit no. 81-02.04.2018.A406, 81-02.04.2021.A060, 81-02.05.40.18.082, and 81-02.04.40.23.VG055). All applicable international, national, and institutional guidelines for the care and use of animals were followed.

T. gondii cyst preparation and infection experiments

ME49 (type II strain) cysts were isolated from the brain of CD1 mice 11 to 19 weeks after infection via Ficoll-Paque gradient centrifugation. Briefly, the murine cerebrum was homogenized by passaging through successively thinner cannulas (smallest size: 23G). After centrifugation (130 × *g*, 5 min, room temperature [RT]), the pellet was resuspended in 20 mL PBS. 10 mL of Ficoll-Paque Plus (GE Healthcare, USA) was carefully layered below the PBS, followed by centrifugation (1,250 × *g*, 25 min, RT) without brakes. Pelleted cysts were washed with PBS, counted (10 cysts per mouse), and lysed with Trypsin-EDTA. Lysis was stopped with the addition of heat-inactivated (56°C, 30 min) fetal calf serum (FCS, Pan Biotech, Germany). After a final wash with PBS and centrifugation (660 × *g*, 10 min, RT), ME49 bradyzoites were resuspended in 0.2 mL PBS per murine recipient. Mice were infected via intraperitoneal injection and weighed and scored daily for the duration of the experiment.

Mouse material preparation and processing

On day 3, 6, and 9 p.i., mice were anesthetized with 100 mg/kg ketamine (Zoetis, USA) and 10 mg/kg xylazine (Elanco, USA). *Peritoneal lavage* was performed by injection (22G) of 5 mL ice-cold PBS (+2% FCS, vol/vol) into the peritoneal cavity, followed by a gentle massage and extraction. Aliquots were prepared for flow cytometry and quantitative real-time PCR (qRT-PCR). *PB/serum*: mice were bled through the *vena cava inferior* (20G). For flow cytometry, 200 µL of PB was immediately added to 50 µL 0.5 M EDTA and stored on ice. After washing with 25 mL PBS (+2% FCS, vol/vol) and centrifugation (470 × *g*, 7 min, 4°C), red blood cells (RBC) were lysed with Erylysis buffer (Morphisto, Germany). Leukocytes were then counted and used for flow cytometry surface staining. Remaining blood was allowed to coagulate for 30 min at room temperature (RT) followed by two centrifugation steps (10 min, 8,000 × *g*) to generate serum. *Bone marrow*: both murine femora were dissected, and BM cells were isolated and pooled via centrifugation. Briefly, femora were cut open at the knee joint side and placed in punctured 0.5 mL tubes that were then placed in 1.5 mL tubes. After centrifugation (12,100 × *g*, 15 sec, RT), the BM supernatant was removed for cytokine measurement. After RBC lysis, remaining leukocytes were counted, and aliquots were prepared for flow cytometry, qRT-PCR, and RNA sequencing.

Cell surface staining for flow cytometry

Cells were stained in U-bottom polystyrene plates and were incubated with Fc-blocking CD16/32 antibody (1:100) in staining buffer (1× PBS with 2 mM EDTA and 2% FCS [vol/vol]) for 30 min at 4°C. Fluorophore-labeled antibodies were prepared in staining buffer, added to cells (final volume: 50 µL), and incubated for 30 min (4°C, light-protected). Cells were then washed, preserved by the addition of 4% paraformaldehyde for 15 min at RT, and analyzed with a BD LSRFortessa II flow cytometer and FlowJo v10.8 software. All antibodies and dyes are listed in Table S1, all identified immune cell populations are listed in Table S2, and all gating strategies are shown in Fig. S1, S5, S6, and S8.

Detection of parasite burden

Bone marrow and peritoneal lavage samples were centrifuged (10,000 × *g*, 5 min, RT), total DNA was isolated from pellets using a DNA isolation kit (Genekam, Germany) according to the manual, and samples were set to 100 ng/µL DNA. TgB1 primer (Forward: 5′-GCT AAA GGC GTC ATT GCT GTT-3′, Reverse: 5′-GGC GGA ACC AAC GGA AAT-3′) and a FAM-probe (5′-FAM-ATC GCA ACG GAG TTC TTC CCA GAC GT-BHQ1-3′) were purchased from Metabion (Germany) to amplify and detect a defined sequence of the 35-fold repetitive B1 gene from *T. gondii*, qRT-PCR was performed on Bio-Rad CFX-96 systems. DNA isolated from a defined number of ME49 tachyzoites (2914 ± 214 /µL) was used to generate a standard curve and calculate parasite loads.

Cytokine measurement

Murine cytokines BAFF, CXCL12, and CXCL13 were measured with a custom-selected bead-based multiplex panel (LEGENDplex from BioLegend, USA). BM^{SN} was used undiluted. Samples were acquired with a BD FACSCanto II or LSRFortessa II and analyzed with Qognit software (BioLegend).

Histology

Liver, lung, spleen, kidney, brain, and femora were harvested from WT and $LT\beta R^{-/-}$ mice, fixed in 4% neutral buffered formalin for 48 hours, and stored in 70% ethanol at 4°C until further processing. 5 µm sections were cut, transferred onto glass slides, and stained with a standard hematoxylin/eosin protocol. Femur samples were decalcified in RDO solution (Apex Engineering, USA) for 1 hour before processing.

Generation of QuantSeq 3′ mRNA-sequencing data

Bone marrow samples of uninfected (d0) and *T. gondii*-infected (ME49, bradyzoites from 10 cysts, i.p.) WT and $LT\beta R^{-/-}$ mice were generated as described and stabilized in RNAprotect Tissue Reagent (Qiagen, Germany). Total RNA was isolated using the RNeasy Plus Mini Kit (Qiagen, Germany), quantified (Qubit RNA HS Assay, Thermo Fisher Scientific, USA), and quality measured by capillary electrophoresis using the Fragment Analyzer and the "Total RNA Standard Sensitivity Assay" (Agilent Technologies, USA). All samples in this study showed high-quality RNA Quality Numbers (RQN mean = 9.8). Library preparation was performed according to the manufacturer's protocol using the Lexogen QuantSeq 3′ mRNA-seq Library Prep Kit FWD with UMI's (Lexogen, Austria). The input amount was 25 ng total RNA. Bead-purified libraries were normalized and finally sequenced on the NextSeq2000 system (Illumina, USA) with a read setup of 1 × 100 bp. The BCL Convert Tool (version 3.8.4) was used to convert the bcl files to fastq files as well as for adapter trimming and demultiplexing.

Analysis of the mRNA-sequencing data

Sequencing data were processed following the recommended protocol on the Lexogen website (https://faqs.lexogen.com/faq/quantseq-with-udi-v2). Using the umi_tools software package (version 1.1.4), we extracted the Unique molecular identifier (UMI)

from the reads of the FASTQ files and removed the adjacent TATA spacer by the "umi_tools extract" command, resulting in FASTQ files with the UMI in the read names (175). Since QuantSeq 3′ mRNA-seq reads contain part of the poly-A tail, we next trimmed any sequenced poly-A sequences and the Lexogen adapter sequences from the read ends, as well as low-quality bases by cutadapt (version 3.5) (176). Reads potentially containing rRNA transcripts were removed using the sortMeRNA tool (version 4.3.7), using the recommended latest database "smr_v4.3_default_db" (177). Data quality was assessed at every step using the tools FASTQC and Multiqc.

For reads alignment, we generated a fused meta-genome with the STAR alignment tool (version 2.7.10 a) (178), combining the genomic sequences and genome annotations of the mouse (GRCm39 ensembl version 111) and toxoplasma (ensemble protists version 55) reference from Ensembl. The reads were then aligned to the fused STAR genome index, which was generated setting the minimal splice site overlap to 99 (--sjdbOverhang 99). Uniquely mapped reads were selected from the BAM files using the samtools software package (version 1.13) (179). Duplicated reads were then removed from the BAM files with umi_tools. Finally, gene count matrices were generated from the BAM files by the featureCount software (version 2.0.3) (180). Differential gene expression analysis was performed on the gene count matrices by a custom R script, using the DESeq2 R package (version 1.44.0) (181). The results of the differential gene expression analysis were then used for GSEA, using the fgsea R package (version 1.30.0) (182).

Statistical analysis

GraphPad Prism software (version 10) was used for data analysis. Symbols represent individual animals, columns represent mean values, and error bars represent the ±standard deviation (SD). Outliers were identified and excluded from the data using the ROUT test (Q = 1%), after which the Shapiro-Wilk test of normality was performed. Parametric data were analyzed using two-way analysis of variance (ANOVA) corrected for multiple comparison using Tukey's *post hoc* test. Nonparametric data were analyzed using the Kruskal-Wallis test followed by Dunn's multiple comparison test.

ACKNOWLEDGMENTS

We thank Julia Mock, Nicole Küpper, Sonja Schavier, and Saskia van Essen-van Dorresteijn for technical assistance. Computational support of the Zentrum für Informations- und Medientechnologie, especially the HPC team (High-Performance Computing) at the Heinrich-Heine University, is acknowledged.

This work was supported by the Jürgen Manchot Foundation (Molecules of Infection IV [MOI IV]). We also acknowledge funding by the German Federal Ministry of Education and Research (Bundesministerium für Bildung und Forschung; Netzwerk Universitätsmedizin, GenSurv/MolTraX), award number 01KX2021.

M.H. performed and analyzed all experiments, except for Fig. 3, 6 and 7, and Fig. S9, S10, and S13, with support from U.R.S. J.P. analyzed and visualized RNA-seq data sets as shown in Fig. 3; Fig. S9 and S10. P.P. and K.K. performed the 3′ RNA sequencing. R.E.T. performed the histological analysis as shown in Fig. 6 and 7; Fig. S13 with support from A.B. K. Pracht and H.-M.J. provided guidance on the identification of B-cell subsets using flow cytometry and on all B-cell-related topics. M.H., U.R.S., and K. Pfeffer designed the study and wrote the manuscript with input from D.D.

AUTHOR AFFILIATIONS

[1]Institute of Medical Microbiology and Hospital Hygiene, Heinrich Heine University, Düsseldorf, Germany
[2]Institute of Virology, Heinrich Heine University, Düsseldorf, Germany
[3]Department Biomolecular Health Sciences, Faculty of Veterinary Medicine, Utrecht University, Utrecht, the Netherlands

[4]Division of Molecular Immunology, Department of Medicine 3-Rheumatology and Immunology, , Universitätsklinikum Erlangen, Friedrich-Alexander-Universität Erlangen-Nürnberg, Erlangen, Germany
[5]Genomics and Transcriptomics Laboratory, Biological and Medical Research Centre (BMFZ), Heinrich Heine University, Düsseldorf, Germany
[6]Institute of Medical Microbiology and Hospital Hygiene, Heinrich Heine University, Düsseldorf, Germany

AUTHOR ORCIDs

Marcel Helle http://orcid.org/0009-0000-5656-3230
Ursula R. Sorg http://orcid.org/0000-0002-0641-6117
Johannes Ptok http://orcid.org/0000-0002-0322-5649
Katharina Pracht http://orcid.org/0000-0002-8943-4897
Patrick Petzsch http://orcid.org/0000-0002-8355-5524
Karl Köhrer http://orcid.org/0000-0003-3644-2022
Daniel Degrandi http://orcid.org/0000-0001-6281-0357
Klaus Pfeffer http://orcid.org/0000-0002-5652-6330

FUNDING

Funder	Grant(s)	Author(s)
Jürgen Manchot Stiftung		Marcel Helle
Bundesministerium für Bildung und Forschung	01KX2021	Johannes Ptok

DATA AVAILABILITY

Raw sequencing data were submitted to the ENA database under accession number PRJNA1177674. Code that was used to analyze the data can be found on github at https://github.com/caggtaagtat/QuantSeq-3-mRNA-sequencing.

ADDITIONAL FILES

The following material is available online.

Supplemental Material

Fig. S1 to S4 (IAI00408-25-S0001.pdf). BM B cell gating strategy (S1), absolute BM B cell numbers (S2), peripheral blood (PB) B cells (S3) and BM plasma cells (BMPCs) (S4).
Fig. S5 to S8 (IAI00408-25-S0002.pdf). BM T cell gating strategy (S5), BM pDC, NK cell and myeloid cells gating strategy (S6), absolute numbers of non-B cells in the BM, PB and PerC (S7) and PerC gating strategy (S8).
Fig. S9 and S10 (IAI00408-25-S0003.pdf). Complete GSEA of LTßR$^{-/-}$ vs WT (S9) and intra-genotype comparisons (S10).
Fig. S11 to S13 (IAI00408-25-S0004.pdf). Absolute PerC B cell numbers and direct B-1a gating (S11), absolute PerC neutrophils and T cells (S12), and histology of kidney sections from WT and LTßR$^{-/-}$ mice (S13).
Supplemental tables (IAI00408-25-S0005.xlsx). Table S1 and S2.

REFERENCES

1. Wimmer N, Huber B, Barabas N, Röhrl J, Pfeffer K, Hehlgans T. 2012. Lymphotoxin β receptor activation on macrophages induces cross-tolerance to TLR4 and TLR9 ligands. J Immunol 188:3426–3433. https://doi.org/10.4049/jimmunol.1103324
2. Wimmer N, Huber B, Wege AK, Barabas N, Röhrl J, Pfeffer K, Hehlgans T. 2012. Lymphotoxin-beta receptor activation on macrophages ameliorates acute DSS-induced intestinal inflammation in a TRIM30α-dependent manner. Mol Immunol 51:128–135. https://doi.org/10.1016/j.molimm.2012.02.118
3. Riffelmacher T, Giles DA, Zahner S, Dicker M, Andreyev AY, McArdle S, Perez-Jeldres T, van der Gracht E, Murray MP, Hartmann N, Tumanov AV, Kronenberg M. 2021. Metabolic activation and colitis pathogenesis is prevented by lymphotoxin β receptor expression in neutrophils.

Mucosal Immunol 14:679–690. https://doi.org/10.1038/s41385-021-00378-7
4. Wang YG, Kim KD, Wang J, Yu P, Fu YX. 2005. Stimulating lymphotoxin beta receptor on the dendritic cells is critical for their homeostasis and expansion. J Immunol 175:6997–7002. https://doi.org/10.4049/jimmunol.175.10.6997
5. Kabashima K, Banks TA, Ansel KM, Lu TT, Ware CF, Cyster JG. 2005. Intrinsic lymphotoxin-beta receptor requirement for homeostasis of lymphoid tissue dendritic cells. Immunity 22:439–450. https://doi.org/10.1016/j.immuni.2005.02.007
6. De Trez C. 2012. Lymphotoxin-beta receptor expression and its related signaling pathways govern dendritic cell homeostasis and function. Immunobiology 217:1250–1258. https://doi.org/10.1016/j.imbio.2012.06.010
7. Ware CF. 2005. Network communications: lymphotoxins, LIGHT, and TNF. Annu Rev Immunol 23:787–819. https://doi.org/10.1146/annurev.immunol.23.021704.115719
8. Hehlgans T, Pfeffer K. 2005. The intriguing biology of the tumour necrosis factor/tumour necrosis factor receptor superfamily: players, rules and the games. Immunology 115:1–20. https://doi.org/10.1111/j.1365-2567.2005.02143.x
9. Ward-Kavanagh LK, Lin WW, Šedý JR, Ware CF. 2016. The TNF receptor superfamily in co-stimulating and co-inhibitory responses. Immunity 44:1005–1019. https://doi.org/10.1016/j.immuni.2016.04.019
10. Dejardin E, Droin NM, Delhase M, Haas E, Cao Y, Makris C, Li ZW, Karin M, Ware CF, Green DR. 2002. The lymphotoxin-beta receptor induces different patterns of gene expression via two NF-kappaB pathways. Immunity 17:525–535. https://doi.org/10.1016/s1074-7613(02)00423-5
11. Fütterer A, Mink K, Luz A, Kosco-Vilbois MH, Pfeffer K. 1998. The lymphotoxin beta receptor controls organogenesis and affinity maturation in peripheral lymphoid tissues. Immunity 9:59–70. https://doi.org/10.1016/s1074-7613(00)80588-9
12. Boulianne B, Porfilio EA, Pikor N, Gommerman JL. 2012. Lymphotoxin-sensitive microenvironments in homeostasis and inflammation. Front Immunol 3:243. https://doi.org/10.3389/fimmu.2012.00243
13. Shou Y, Koroleva E, Spencer CM, Shein SA, Korchagina AA, Yusoof KA, Parthasarathy R, Leadbetter EA, Akopian AN, Muñoz AR, Tumanov AV. 2021. Redefining the role of lymphotoxin beta receptor in the maintenance of lymphoid organs and immune cell homeostasis in adulthood. Front Immunol 12:712632. https://doi.org/10.3389/fimmu.2021.712632
14. Ngo V.N., Cornall RJ, Cyster JG. 2001. Splenic T zone development is B cell dependent. J Exp Med 194:1649–1660. https://doi.org/10.1084/jem.194.11.1649
15. Ngo VN, Korner H, Gunn MD, Schmidt KN, Riminton DS, Cooper MD, Browning JL, Sedgwick JD, Cyster JG. 1999. Lymphotoxin α/β and tumor necrosis factor are required for stromal cell expression of homing chemokines in B and T cell areas of the spleen. J Exp Med 189:403–412. https://doi.org/10.1084/jem.189.2.403
16. Myers RC, King RG, Carter RH, Justement LB. 2013. Lymphotoxin α1β2 expression on B cells is required for follicular dendritic cell activation during the germinal center response. Eur J Immunol 43:348–359. https://doi.org/10.1002/eji.201242471
17. Vu F, Dianzani U, Ware CF, Mak T, Gommerman JL. 2008. ICOS, CD40, and lymphotoxin beta receptors signal sequentially and interdependently to initiate a germinal center reaction. J Immunol 180:2284–2293. https://doi.org/10.4049/jimmunol.180.4.2284
18. Wu Q, Wang Y, Wang J, Hedgeman EO, Browning JL, Fu YX. 1999. The requirement of membrane lymphotoxin for the presence of dendritic cells in lymphoid tissues. J Exp Med 190:629–638. https://doi.org/10.1084/jem.190.5.629
19. Fu YX, Huang G, Wang Y, Chaplin DD. 1998. B lymphocytes induce the formation of follicular dendritic cell clusters in a lymphotoxin alpha-dependent fashion. J Exp Med 187:1009–1018. https://doi.org/10.1084/jem.187.7.1009
20. Zindl CL, Kim TH, Zeng M, Archambault AS, Grayson MH, Choi K, Schreiber RD, Chaplin DD. 2009. The lymphotoxin LTalpha(1)beta(2) controls postnatal and adult spleen marginal sinus vascular structure and function. Immunity 30:408–420. https://doi.org/10.1016/j.immuni.2009.01.010
21. Camara A, Lavanant AC, Abe J, Desforges HL, Alexandre YO, Girardi E, Igamberdieva Z, Asano K, Tanaka M, Hehlgans T, Pfeffer K, Pfeffer S, Mueller SN, Stein JV, Mueller CG. 2022. CD169^{+} macrophages in lymph node and spleen critically depend on dual RANK and LTbetaR signaling. Proc Natl Acad Sci USA 119:e2108540119. https://doi.org/10.1073/pnas.2108540119
22. Elewaut D, Brossay L, Santee SM, Naidenko OV, Burdin N, De Winter H, Matsuda J, Ware CF, Cheroutre H, Kronenberg M. 2000. Membrane lymphotoxin is required for the development of different subpopulations of NK T cells. J Immunol 165:671–679. https://doi.org/10.4049/jimmunol.165.2.671
23. Franki AS, Van Beneden K, Dewint P, Hammond KJL, Lambrecht S, Leclercq G, Kronenberg M, Deforce D, Elewaut D. 2006. A unique lymphotoxin {alpha}beta-dependent pathway regulates thymic emigration of V{alpha}14 invariant natural killer T cells. Proc Natl Acad Sci USA 103:9160–9165. https://doi.org/10.1073/pnas.0508892103
24. Iizuka K, Chaplin DD, Wang Y, Wu Q, Pegg LE, Yokoyama WM, Fu YX. 1999. Requirement for membrane lymphotoxin in natural killer cell development. Proc Natl Acad Sci USA 96:6336–6340. https://doi.org/10.1073/pnas.96.11.6336
25. Tersteegen A, Sorg UR, Virgen-Slane R, Helle M, Petzsch P, Dunay IR, Köhrer K, Degrandi D, Ware CF, Pfeffer K. 2021. Lymphotoxin β receptor: a crucial role in innate and adaptive immune responses against *Toxoplasma gondii*. Infect Immun 89:e00026-21. https://doi.org/10.1128/IAI.00026-21
26. Borelli A, Irla M. 2021. Lymphotoxin: from the physiology to the regeneration of the thymic function. Cell Death Differ 28:2305–2314. https://doi.org/10.1038/s41418-021-00834-8
27. Boehm T, Scheu S, Pfeffer K, Bleul CC. 2003. Thymic medullary epithelial cell differentiation, thymocyte emigration, and the control of autoimmunity require lympho-epithelial cross talk via LTbetaR. J Exp Med 198:757–769. https://doi.org/10.1084/jem.20030794
28. Cosway EJ, Lucas B, James KD, Parnell SM, Carvalho-Gaspar M, White AJ, Tumanov AV, Jenkinson WE, Anderson G. 2017. Redefining thymus medulla specialization for central tolerance. J Exp Med 214:3183–3195. https://doi.org/10.1084/jem.20171000
29. Behnke K, Sorg UR, Gabbert HE, Pfeffer K. 2017. The lymphotoxin beta receptor is essential for upregulation of IFN-induced guanylate-binding proteins and survival after *Toxoplasma gondii* infection. Mediators Inflamm 7375818. https://doi.org/10.1155/2017/7375818
30. Banks TA, Rickert S, Ware CF. 2006. Restoring immune defenses via lymphotoxin signaling: lessons from cytomegalovirus. Immunol Res 34:243–254. https://doi.org/10.1385/IR:34:3:243
31. Ehlers S, Hölscher C, Scheu S, Tertilt C, Hehlgans T, Suwinski J, Endres R, Pfeffer K. 2003. The lymphotoxin beta receptor is critically involved in controlling infections with the intracellular pathogens *Mycobacterium tuberculosis* and *Listeria monocytogenes*. J Immunol 170:5210–5218. https://doi.org/10.4049/jimmunol.170.10.5210
32. Jin L, Guo X, Shen C, Hao X, Sun P, Li P, Xu T, Hu C, Rose O, Zhou H, Yang M, Qin CF, Guo J, Peng H, Zhu M, Cheng G, Qi X, Lai R. 2018. Salivary factor LTRIN from *Aedes aegypti* facilitates the transmission of Zika virus by interfering with the lymphotoxin-β receptor. Nat Immunol 19:342–353. https://doi.org/10.1038/s41590-018-0063-9
33. Puglielli MT, Browning JL, Brewer AW, Schreiber RD, Shieh WJ, Altman JD, Oldstone MB, Zaki SR, Ahmed R. 1999. Reversal of virus-induced systemic shock and respiratory failure by blockade of the lymphotoxin pathway. Nat Med 5:1370–1374. https://doi.org/10.1038/70938
34. Spahn TW, Maaser C, Eckmann L, Heidemann J, Lügering A, Newberry R, Domschke W, Herbst H, Kucharzik T. 2004. The lymphotoxin-beta receptor is critical for control of murine *Citrobacter rodentium*-induced colitis. Gastroenterology 127:1463–1473. https://doi.org/10.1053/j.gastro.2004.08.022
35. Fernandes MT, Dejardin E, dos Santos NR. 2016. Context-dependent roles for lymphotoxin-β receptor signaling in cancer development. Biochim Biophys Acta 1865:204–219. https://doi.org/10.1016/j.bbcan.2016.02.005
36. Wolf MJ, Seleznik GM, Zeller N, Heikenwalder M. 2010. The unexpected role of lymphotoxin beta receptor signaling in carcinogenesis: from lymphoid tissue formation to liver and prostate cancer development. Oncogene 29:5006–5018. https://doi.org/10.1038/onc.2010.260
37. Seleznik G, Seeger H, Bauer J, Fu K, Czerkowicz J, Papandile A, Poreci U, Rabah D, Ranger A, Cohen CD, Lindenmeyer M, Chen J, Edenhofer I, Anders HJ, Lech M, Wüthrich RP, Ruddle NH, Moeller MJ, Kozakowski N, Regele H, Browning JL, Heikenwalder M, Segerer S. 2016. The lymphotoxin β receptor is a potential therapeutic target in renal inflammation. Kidney Int 89:113–126. https://doi.org/10.1038/ki.2015.280

38. Zhang G, Feizi N, Zhao D, Halesha L, Williams AL, Randhawa PS, Abou-Daya KI, Oberbarnscheidt MH. 2024. Lymphotoxin β receptor and tertiary lymphoid organs shape acute and chronic allograft rejection. JCI Insight 9:e177555. https://doi.org/10.1172/jci.insight.177555
39. Robert-Gangneux F, Dardé M-L. 2012. Epidemiology of and diagnostic strategies for toxoplasmosis. Clin Microbiol Rev 25:264–296. https://doi.org/10.1128/CMR.05013-11
40. Martorelli Di Genova B, Wilson SK, Dubey JP, Knoll LJ. 2019. Intestinal delta-6-desaturase activity determines host range for Toxoplasma sexual reproduction. PLoS Biol 17:e3000364. https://doi.org/10.1371/journal.pbio.3000364
41. English ED, Striepen B. 2019. The cat is out of the bag: how parasites know their hosts. PLoS Biol 17:e3000446. https://doi.org/10.1371/journal.pbio.3000446
42. Daher D, Shaghlil A, Sobh E, Hamie M, Hassan ME, Moumneh MB, Itani S, El Hajj R, Tawk L, El Sabban M, El Hajj H. 2021. Comprehensive overview of *Toxoplasma gondii*-induced and associated diseases. Pathogens 10:1351. https://doi.org/10.3390/pathogens10111351
43. Zhang Y, Li D, Lu S, Zheng B. 2022. Toxoplasmosis vaccines: what we have and where to go? NPJ Vaccines 7:131. https://doi.org/10.1038/s41541-022-00563-0
44. Khan IA, Moretto M. 2022. Immune responses to *Toxoplasma gondii*. Curr Opin Immunol 77:102226. https://doi.org/10.1016/j.coi.2022.102226
45. Iwasaki A, Medzhitov R. 2010. Regulation of adaptive immunity by the innate immune system. Science 327:291–295. https://doi.org/10.1126/science.1183021
46. Sasai M, Yamamoto M. 2019. Innate, adaptive, and cell-autonomous immunity against Toxoplasma gondii infection. Exp Mol Med 51:1–10. https://doi.org/10.1038/s12276-019-0353-9
47. Yarovinsky F. 2014. Innate immunity to *Toxoplasma gondii* infection. Nat Rev Immunol 14:109–121. https://doi.org/10.1038/nri3598
48. Gazzinelli RT, Hieny S, Wynn TA, Wolf S, Sher A. 1993. Interleukin 12 is required for the T-lymphocyte-independent induction of interferon gamma by an intracellular parasite and induces resistance in T-cell-deficient hosts. Proc Natl Acad Sci USA 90:6115–6119. https://doi.org/10.1073/pnas.90.13.6115
49. Hunter CA, Subauste CS, Van Cleave VH, Remington JS. 1994. Production of gamma interferon by natural killer cells from *Toxoplasma gondii*-infected SCID mice: regulation by interleukin-10, interleukin-12, and tumor necrosis factor alpha. Infect Immun 62:2818–2824. https://doi.org/10.1128/iai.62.7.2818-2824.1994
50. Hou B, Benson A, Kuzmich L, DeFranco AL, Yarovinsky F. 2011. Critical coordination of innate immune defense against *Toxoplasma gondii* by dendritic cells responding via their Toll-like receptors. Proc Natl Acad Sci USA 108:278–283. https://doi.org/10.1073/pnas.1011549108
51. Wilson DC, Matthews S, Yap GS. 2008. IL-12 signaling drives CD8+ T cell IFN-gamma production and differentiation of KLRG1+ effector subpopulations during *Toxoplasma gondii* Infection. J Immunol 180:5935–5945. https://doi.org/10.4049/jimmunol.180.9.5935
52. Yap G, Pesin M, Sher A. 2000. Cutting edge: IL-12 is required for the maintenance of IFN-gamma production in T cells mediating chronic resistance to the intracellular pathogen, *Toxoplasma gondii*. J Immunol 165:628–631. https://doi.org/10.4049/jimmunol.165.2.628
53. Spits H, Bernink JH, Lanier L. 2016. NK cells and type 1 innate lymphoid cells: partners in host defense. Nat Immunol 17:758–764. https://doi.org/10.1038/ni.3482
54. Dunay IR, Diefenbach A. 2018. Group 1 innate lymphoid cells in *Toxoplasma gondii* infection. Parasite Immunol 40. https://doi.org/10.1111/pim.12516
55. Steffen J, Ehrentraut S, Bank U, Biswas A, Figueiredo CA, Hölsken O, Düsedau HP, Dovhan V, Knop L, Thode J, Romero-Suárez S, Duarte CI, Gigley J, Romagnani C, Diefenbach A, Klose CSN, Schüler T, Dunay IR. 2022. Type 1 innate lymphoid cells regulate the onset of *Toxoplasma gondii*-induced neuroinflammation. Cell Rep 38:110564. https://doi.org/10.1016/j.celrep.2022.110564
56. López-Yglesias AH, Burger E, Camanzo E, Martin AT, Araujo AM, Kwok SF, Yarovinsky F. 2021. T-bet-dependent ILC1- and NK cell-derived IFN-γ mediates cDC1-dependent host resistance against *Toxoplasma gondii*. PLoS Pathog 17:e1008299. https://doi.org/10.1371/journal.ppat.1008299
57. Suzuki Y, Orellana MA, Schreiber RD, Remington JS. 1988. Interferon-gamma: the major mediator of resistance against *Toxoplasma gondii*. Science 240:516–518. https://doi.org/10.1126/science.3128869
58. Yap GS, Sher A. 1999. Cell-mediated immunity to *Toxoplasma gondii*: initiation, regulation and effector function. Immunobiology 201:240–247. https://doi.org/10.1016/S0171-2985(99)80064-3
59. Haldar AK, Saka HA, Piro AS, Dunn JD, Henry SC, Taylor GA, Frickel EM, Valdivia RH, Coers J. 2013. IRG and GBP host resistance factors target aberrant, "non-self" vacuoles characterized by the missing of "self" IRGM proteins. PLoS Pathog 9:e1003414. https://doi.org/10.1371/journal.ppat.1003414
60. Henry SC, Daniell XG, Burroughs AR, Indaram M, Howell DN, Coers J, Starnbach MN, Hunn JP, Howard JC, Feng CG, Sher A, Taylor GA. 2009. Balance of Irgm protein activities determines IFN-gamma-induced host defense. J Leukoc Biol 85:877–885. https://doi.org/10.1189/jlb.1008599
61. Hunn JP, Koenen-Waisman S, Papic N, Schroeder N, Pawlowski N, Lange R, Kaiser F, Zerrahn J, Martens S, Howard JC. 2008. Regulatory interactions between IRG resistance GTPases in the cellular response to *Toxoplasma gondii*. EMBO J 27:2495–2509. https://doi.org/10.1038/emboj.2008.176
62. Khaminets A, Hunn JP, Könen-Waisman S, Zhao YO, Preukschat D, Coers J, Boyle JP, Ong Y-C, Boothroyd JC, Reichmann G, Howard JC. 2010. Coordinated loading of IRG resistance GTPases on to the *Toxoplasma gondii* parasitophorous vacuole. Cell Microbiol 12:939–961. https://doi.org/10.1111/j.1462-5822.2010.01443.x
63. Martens S, Parvanova I, Zerrahn J, Griffiths G, Schell G, Reichmann G, Howard JC. 2005. Disruption of *Toxoplasma gondii* parasitophorous vacuoles by the mouse p47-resistance GTPases. PLoS Pathog 1:e24. https://doi.org/10.1371/journal.ppat.0010024
64. Degrandi D, Kravets E, Konermann C, Beuter-Gunia C, Klümpers V, Lahme S, Rasch E, Mausberg AK, Beer-Hammer S, Pfeffer K. 2013. Murine guanylate binding protein 2 (mGBP2) controls *Toxoplasma gondii* replication. Proc Natl Acad Sci USA 110:294–299. https://doi.org/10.1073/pnas.1205635110
65. Kravets E, Degrandi D, Weidtkamp-Peters S, Ries B, Konermann C, Felekyan S, Dargazanli JM, Praefcke GJK, Seidel CAM, Schmitt L, Smits SHJ, Pfeffer K. 2012. The GTPase activity of murine guanylate-binding protein 2 (mGBP2) controls the intracellular localization and recruitment to the parasitophorous vacuole of *Toxoplasma gondii*. J Biol Chem 287:27452–27466. https://doi.org/10.1074/jbc.M112.379636
66. Selleck EM, Fentress SJ, Beatty WL, Degrandi D, Pfeffer K, Virgin HW, 4th, Macmicking JD, Sibley LD. 2013. Guanylate-binding protein 1 (Gbp1) contributes to cell-autonomous immunity against *Toxoplasma gondii*. PLoS Pathog 9:e1003320. https://doi.org/10.1371/journal.ppat.1003320
67. Steffens N, Beuter-Gunia C, Kravets E, Reich A, Legewie L, Pfeffer K, Degrandi D. 2020. Essential Role of mGBP7 for Survival of *Toxoplasma gondii* Infection. mBio 11:e02993-19. https://doi.org/10.1128/mBio.02993-19
68. Yamamoto M, Okuyama M, Ma JS, Kimura T, Kamiyama N, Saiga H, Ohshima J, Sasai M, Kayama H, Okamoto T, Huang DCS, Soldati-Favre D, Horie K, Takeda J, Takeda K. 2012. A cluster of interferon-γ-inducible p65 GTPases plays a critical role in host defense against *Toxoplasma gondii*. Immunity 37:302–313. https://doi.org/10.1016/j.immuni.2012.06.009
69. El Bissati K, Krishack PA, Zhou Y, Weber CR, Lykins J, Jankovic D, Edelblum KL, Fraczek L, Grover H, Chentoufi AA, Singh G, Reardon C, Dubey JP, Reed S, Alexander J, Sidney J, Sette A, Shastri N, McLeod R. 2023. CD4+ T cell responses to *Toxoplasma gondii* are a double-edged sword. Vaccines 11:1485. https://doi.org/10.3390/vaccines11091485
70. Gazzinelli RT, Wysocka M, Hieny S, Scharton-Kersten T, Cheever A, Kühn R, Müller W, Trinchieri G, Sher A. 1996. In the absence of endogenous IL-10, mice acutely infected with *Toxoplasma gondii* succumb to a lethal immune response dependent on CD4+ T cells and accompanied by overproduction of IL-12, IFN-gamma and TNF-alpha. J Immunol 157:798–805. https://doi.org/10.4049/jimmunol.157.2.798
71. López-Yglesias AH, Burger E, Araujo A, Martin AT, Yarovinsky F. 2018. T-bet-independent Th1 response induces intestinal immunopathology during *Toxoplasma gondii* infection. Mucosal Immunol 11:921–931. https://doi.org/10.1038/mi.2017.102
72. Olguín JE, Fernández J, Salinas N, Juárez I, Rodriguez-Sosa M, Campuzano J, Castellanos C, Saavedra R. 2015. Adoptive transfer of CD4(+)Foxp3(+) regulatory T cells to C57BL/6J mice during acute infection with *Toxoplasma gondii* down modulates the exacerbated Th1 immune response. Microbes Infect 17:586–595. https://doi.org/10.1016/j.micinf.2015.04.002
73. Saraav I, Cervantes-Barragan L, Olias P, Fu Y, Wang Q, Wang L, Wang Y, Mack M, Baldridge MT, Stappenbeck T, Colonna M, Sibley LD. 2021.

Chronic *Toxoplasma gondii* infection enhances susceptibility to colitis. Proc Natl Acad Sci USA 118:e2106730118. https://doi.org/10.1073/pnas.2106730118
74. Warunek J, Jin RM, Blair SJ, Garis M, Marzullo B, Wohlfert EA. 2021. Tbet expression by regulatory T cells is needed to protect against Th1-mediated immunopathology during *Toxoplasma* infection in mice. Immunohorizons 5:931–943. https://doi.org/10.4049/immunohorizons.2100080
75. Zhang ZX, Yang L, Young KJ, DuTemple B, Zhang L. 2000. Identification of a previously unknown antigen-specific regulatory T cell and its mechanism of suppression. Nat Med 6:782–789. https://doi.org/10.1038/77513
76. Merims S, Li X, Joe B, Dokouhaki P, Han M, Childs RW, Wang ZY, Gupta V, Minden MD, Zhang L. 2011. Anti-leukemia effect of *ex vivo* expanded DNT cells from AML patients: a potential novel autologous T-cell adoptive immunotherapy. Leukemia 25:1415–1422. https://doi.org/10.1038/leu.2011.99
77. Sykes M. 1990. Unusual T cell populations in adult murine bone marrow. Prevalence of CD3+CD4-CD8- and alpha beta TCR+NK1.1+ cells. J Immunol 145:3209–3215. https://doi.org/10.4049/jimmunol.145.10.3209
78. Wu Z, Zheng Y, Sheng J, Han Y, Yang Y, Pan H, Yao J. 2022. CD3(+)CD4(-)CD8(-) (Double-Negative) T cells in inflammation, immune disorders and cancer. Front Immunol 13:816005. https://doi.org/10.3389/fimmu.2022.816005
79. Hu Z, Yang M, Chen H, He C, Lin Z, Yang X, Li H, Shen W, Lu D, Xu X. 2023. Double-negative T cells: a promising avenue of adoptive cell therapy in transplant oncology. J Zhejiang Univ Sci B 24:387–396. https://doi.org/10.1631/jzus.B2200528
80. Li H, Tsokos GC. 2021. Double-negative T cells in autoimmune diseases. Curr Opin Rheumatol 33:163–172. https://doi.org/10.1097/BOR.0000000000000778
81. Martina MN, Noel S, Saxena A, Rabb H, Hamad ARA. 2015. Double negative (DN) αβ T cells: misperception and overdue recognition. Immunol Cell Biol 93:305–310. https://doi.org/10.1038/icb.2014.99
82. Vercammen M, Scorza T, El Bouhdidi A, Van Beeck K, Carlier Y, Dubremetz JF, Verschueren H. 1999. Opsonization of *Toxoplasma gondii* tachyzoites with nonspecific immunoglobulins promotes their phagocytosis by macrophages and inhibits their proliferation in nonphagocytic cells in tissue culture. Parasite Immunol 21:555–563. https://doi.org/10.1046/j.1365-3024.1999.00256.x
83. Kang H, Remington JS, Suzuki Y. 2000. Decreased resistance of B cell-deficient mice to infection with *Toxoplasma gondii* despite unimpaired expression of IFN-gamma, TNF-alpha, and inducible nitric oxide synthase. J Immunol 164:2629–2634. https://doi.org/10.4049/jimmunol.164.5.2629
84. Sayles PC, Gibson GW, Johnson LL. 2000. B cells are essential for vaccination-induced resistance to virulent *Toxoplasma gondii*. Infect Immun 68:1026–1033. https://doi.org/10.1128/IAI.68.3.1026-1033.2000
85. Johnson LL, Sayles PC. 2002. Deficient humoral responses underlie susceptibility to *Toxoplasma gondii* in CD4-deficient mice. Infect Immun 70:185–191. https://doi.org/10.1128/IAI.70.1.185-191.2002
86. Chen M, Mun HS, Piao LX, Aosai F, Norose K, Mohamed RM, Belal US, Fang H, Ahmed AK, Kang HK, Matsuzaki G, Kitamura D, Yano A. 2003. Induction of protective immunity by primed B-1 cells in *Toxoplasma gondii* -infected B cell-deficient mice. Microbiol Immunol 47:997–1003. https://doi.org/10.1111/j.1348-0421.2003.tb03460.x
87. Johnson LL, Lanthier P, Hoffman J, Chen W. 2004. Vaccination protects B cell-deficient mice against an oral challenge with mildly virulent *Toxoplasma gondii*. Vaccine 22:4054–4061. https://doi.org/10.1016/j.vaccine.2004.03.056
88. Couper KN, Roberts CW, Brombacher F, Alexander J, Johnson LL. 2005. *Toxoplasma gondii*-specific immunoglobulin M limits parasite dissemination by preventing host cell invasion. Infect Immun 73:8060–8068. https://doi.org/10.1128/IAI.73.12.8060-8068.2005
89. Souza SP, Splitt SD, Sànchez-Arcila JC, Alvarez JA, Wilson JN, Wizzard S, Luo Z, Baumgarth N, Jensen KDC. 2021. Genetic mapping reveals Nfkbid as a central regulator of humoral immunity to *Toxoplasma gondii*. PLoS Pathog 17:e1010081. https://doi.org/10.1371/journal.ppat.1010081
90. Kantor AB, Stall AM, Adams S, Herzenberg LA, Herzenberg LA. 1992. Differential development of progenitor activity for three B-cell lineages. Proc Natl Acad Sci USA 89:3320–3324. https://doi.org/10.1073/pnas.89.8.3320
91. Cariappa A, Chase C, Liu H, Russell P, Pillai S. 2007. Naive recirculating B cells mature simultaneously in the spleen and bone marrow. Blood 109:2339–2345. https://doi.org/10.1182/blood-2006-05-021089
92. Shahaf G, Zisman-Rozen S, Benhamou D, Melamed D, Mehr R. 2016. B cell development in the bone marrow Is regulated by homeostatic feedback exerted by mature B cells. Front Immunol 7:77. https://doi.org/10.3389/fimmu.2016.00077
93. Baumgarth N. 2011. The double life of a B-1 cell: self-reactivity selects for protective effector functions. Nat Rev Immunol 11:34–46. https://doi.org/10.1038/nri2901
94. Kantor AB, Merrill CE, Herzenberg LA, Hillson JL. 1997. An unbiased analysis of V(H)-D-J(H) sequences from B-1a, B-1b, and conventional B cells. J Immunol 158:1175–1186. https://doi.org/10.4049/jimmunol.158.3.1175
95. Martin F, Oliver AM, Kearney JF. 2001. Marginal zone and B1 B cells unite in the early response against T-independent blood-borne particulate antigens. Immunity 14:617–629. https://doi.org/10.1016/s1074-7613(01)00129-7
96. Haas KM, Poe JC, Steeber DA, Tedder TF. 2005. B-1a and B-1b cells exhibit distinct developmental requirements and have unique functional roles in innate and adaptive immunity to *S. pneumoniae*. Immunity 23:7–18. https://doi.org/10.1016/j.immuni.2005.04.011
97. Choi YS, Dieter JA, Rothaeusler K, Luo Z, Baumgarth N. 2012. B-1 cells in the bone marrow are a significant source of natural IgM. Eur J Immunol 42:120–129. https://doi.org/10.1002/eji.201141890
98. Holodick NE, Rodríguez-Zhurbenko N, Hernández AM. 2017. Defining Natural Antibodies. Front Immunol 8:872. https://doi.org/10.3389/fimmu.2017.00872
99. Smith FL, Baumgarth N. 2019. B-1 cell responses to infections. Curr Opin Immunol 57:23–31. https://doi.org/10.1016/j.coi.2018.12.001
100. Chen M, Aosai F, Mun HS, Norose K, Hata H, Yano A. 2000. Anti-HSP70 autoantibody formation by B-1 cells in *Toxoplasma gondii*-infected mice. Infect Immun 68:4893–4899. https://doi.org/10.1128/IAI.68.9.4893-4899.2000
101. Chen M, Aosai F, Norose K, Mun HS, Yano A. 2003. The role of anti-HSP70 autoantibody-forming VH1-JH1 B-1 cells in *Toxoplasma gondii*-infected mice. Int Immunol 15:39–47. https://doi.org/10.1093/intimm/dxg004
102. Masihi KN, Werner H. 1977. Suppression and enhancement of humoral immune response to *Toxoplasma gondii* by passive antibody. Experientia 33:1586–1587. https://doi.org/10.1007/BF01934012
103. Strickland GT, Sayles PC. 1977. Depressed antibody responses to a thymus-dependent antigen in toxoplasmosis. Infect Immun 15:184–190. https://doi.org/10.1128/iai.15.1.184-190.1977
104. Kobayashi A, Suzuki Y. 1987. Suppression of antibody responses by *Toxoplasma* infection in mice. Zentralbl Bakteriol Mikrobiol Hyg A 264:312–318. https://doi.org/10.1016/S0176-6724(87)80049-4
105. Amezcua Vesely MC, Bermejo DA, Montes CL, Acosta-Rodríguez EV, Gruppi A. 2012. B-cell response during protozoan parasite infections. J Parasitol Res 2012:362131. https://doi.org/10.1155/2012/362131
106. Lim VY, Zehentmeier S, Fistonich C, Pereira JP. 2017. A chemoattractant-guided walk through lymphopoiesis: from hematopoietic stem cells to mature B lymphocytes. Adv Immunol 134:47–88. https://doi.org/10.1016/bs.ai.2017.02.001
107. Ueda Y, Yang K, Foster SJ, Kondo M, Kelsoe G. 2004. Inflammation controls B lymphopoiesis by regulating chemokine CXCL12 expression. J Exp Med 199:47–58. https://doi.org/10.1084/jem.20031104
108. Pracht K, Meinzinger J, Daum P, Schulz SR, Reimer D, Hauke M, Roth E, Mielenz D, Berek C, Côrte‐Real J, Jäck H, Schuh W. 2017. A new staining protocol for detection of murine antibody‐secreting plasma cell subsets by flow cytometry. Eur J Immunol 47:1389–1392. https://doi.org/10.1002/eji.201747019
109. Kim TJ, Upadhyay V, Kumar V, Lee KM, Fu YX. 2014. Innate lymphoid cells facilitate NK cell development through a lymphotoxin-mediated stromal microenvironment. J Exp Med 211:1421–1431. https://doi.org/10.1084/jem.20131501
110. Summers-deLuca LE, McCarthy DD, Cosovic B, Ward LA, Lo CC, Scheu S, Pfeffer K, Gommerman JL. 2007. Expression of lymphotoxin-αβ on antigen-specific T cells is required for DC function. J Exp Med 204:1071–1081. https://doi.org/10.1084/jem.20061968
111. Wang G, Abadía-Molina AC, Berger SB, Romero X, O'Keeffe MS, Rojas-Barros DI, Aleman M, Liao G, Maganto-García E, Fresno M, Wang N, Detre C, Terhorst C. 2012. Cutting edge: slamf8 is a negative regulator

of Nox2 activity in macrophages. J Immunol 188:5829–5832. https://doi.org/10.4049/jimmunol.1102620
112. Li F, Yang M, Wang L, Williamson I, Tian F, Qin M, Shah PK, Sharifi BG. 2012. Autofluorescence contributes to false-positive intracellular Foxp3 staining in macrophages: A lesson learned from flow cytometry. J Immunol Methods 386:101–107. https://doi.org/10.1016/j.jim.2012.08.014
113. Martin AT, Giri S, Safronova A, Eliseeva SI, Kwok SF, Yarovinsky F. 2024. Parasite-induced IFN-γ regulates host defense via CD115 and mTOR-dependent mechanism of tissue-resident macrophage death. PLoS Pathog 20:e1011502. https://doi.org/10.1371/journal.ppat.1011502
114. Aziz M, Holodick NE, Rothstein TL, Wang P. 2015. The role of B-1 cells in inflammation. Immunol Res 63:153–166. https://doi.org/10.1007/s12026-015-8708-3
115. Baumgarth N. 2016. B-1 cell heterogeneity and the regulation of natural and antigen-induced IgM production. Front Immunol 7:324. https://doi.org/10.3389/fimmu.2016.00324
116. Ansel KM, Harris RBS, Cyster JG. 2002. CXCL13 is required for B1 cell homing, natural antibody production, and body cavity immunity. Immunity 16:67–76. https://doi.org/10.1016/S1074-7613(01)00257-6
117. Ha S, Tsuji M, Suzuki K, Meek B, Yasuda N, Kaisho T, Fagarasan S. 2006. Regulation of B1 cell migration by signals through Toll-like receptors. J Exp Med 203:2541–2550. https://doi.org/10.1084/jem.20061041
118. Chin RK, Lo JC, Kim O, Blink SE, Christiansen PA, Peterson P, Wang Y, Ware C, Fu YX. 2003. Lymphotoxin pathway directs thymic Aire expression. Nat Immunol 4:1121–1127. https://doi.org/10.1038/ni982
119. Lindsley RC, Thomas M, Srivastava B, Allman D. 2007. Generation of peripheral B cells occurs via two spatially and temporally distinct pathways. Blood 109:2521–2528. https://doi.org/10.1182/blood-2006-04-018085
120. Cariappa A, Mazo IB, Chase C, Shi HN, Liu H, Li Q, Rose H, Leung H, Cherayil BJ, Russell P, von Andrian U, Pillai S. 2005. Perisinusoidal B cells in the bone marrow participate in T-independent responses to blood-borne microbes. Immunity 23:397–407. https://doi.org/10.1016/j.immuni.2005.09.004
121. Pillai S, Cariappa A. 2009. The bone marrow perisinusoidal niche for recirculating B cells and the positive selection of bone marrow-derived B lymphocytes. Immunol Cell Biol 87:16–19. https://doi.org/10.1038/icb.2008.89
122. Sapoznikov A, Pewzner-Jung Y, Kalchenko V, Krauthgamer R, Shachar I, Jung S. 2008. Perivascular clusters of dendritic cells provide critical survival signals to B cells in bone marrow niches. Nat Immunol 9:388–395. https://doi.org/10.1038/ni1571
123. Kang HS, Chin RK, Wang Y, Yu P, Wang J, Newell KA, Fu YX. 2002. Signaling via LTβR on the lamina propria stromal cells of the gut is required for IgA production. Nat Immunol 3:576–582. https://doi.org/10.1038/ni795
124. Ansel KM, Ngo VN, Hyman PL, Luther SA, Förster R, Sedgwick JD, Browning JL, Lipp M, Cyster JG. 2000. A chemokine-driven positive feedback loop organizes lymphoid follicles. Nature 406:309–314. https://doi.org/10.1038/35018581
125. Browning JL, Allaire N, Ngam-Ek A, Notidis E, Hunt J, Perrin S, Fava RA. 2005. Lymphotoxin-beta receptor signaling is required for the homeostatic control of HEV differentiation and function. Immunity 23:539–550. https://doi.org/10.1016/j.immuni.2005.10.002
126. Piao W, Kasinath V, Saxena V, Lakhan R, Iyyathurai J, Bromberg JS. 2021. LTβR signaling controls lymphatic migration of immune cells. Cells 10:747. https://doi.org/10.3390/cells10040747
127. Madge LA, Kluger MS, Orange JS, May MJ. 2008. Lymphotoxin-alpha 1 beta 2 and LIGHT induce classical and noncanonical NF-kappa B-dependent proinflammatory gene expression in vascular endothelial cells. J Immunol 180:3467–3477. https://doi.org/10.4049/jimmunol.180.5.3467
128. Lucas B, James KD, Cosway EJ, Parnell SM, Tumanov AV, Ware CF, Jenkinson WE, Anderson G. 2016. Lymphotoxin β receptor controls T cell progenitor entry to the thymus. J Immunol 197:2665–2672. https://doi.org/10.4049/jimmunol.1601189
129. Zhu M, Chin RK, Tumanov AV, Liu X, Fu YX. 2007. Lymphotoxin beta receptor is required for the migration and selection of autoreactive T cells in thymic medulla. J Immunol 179:8069–8075. https://doi.org/10.4049/jimmunol.179.12.8069
130. Shi Y, Wu W, Chai Q, Li Q, Hou Y, Xia H, Ren B, Xu H, Guo X, Jin C, Lv M, Wang Z, Fu YX, Zhu M. 2016. LTβR controls thymic portal endothelial cells for haematopoietic progenitor cell homing and T-cell regeneration. Nat Commun 7:12369. https://doi.org/10.1038/ncomms12369
131. Mouri Y, Yano M, Shinzawa M, Shimo Y, Hirota F, Nishikawa Y, Nii T, Kiyonari H, Abe T, Uehara H, Izumi K, Tamada K, Chen L, Penninger JM, Inoue J, Akiyama T, Matsumoto M. 2011. Lymphotoxin signal promotes thymic organogenesis by eliciting RANK expression in the embryonic thymic stroma. J Immunol 186:5047–5057. https://doi.org/10.4049/jimmunol.1003533
132. James KD, Cosway EJ, Lucas B, White AJ, Parnell SM, Carvalho-Gaspar M, Tumanov AV, Anderson G, Jenkinson WE. 2018. Endothelial cells act as gatekeepers for LTβR-dependent thymocyte emigration. J Exp Med 215:2984–2993. https://doi.org/10.1084/jem.20181345
133. Hoffmann A, Kerr S, Jellusova J, Zhang J, Weisel F, Wellmann U, Winkler TH, Kneitz B, Crocker PR, Nitschke L. 2007. Siglec-G is a B1 cell-inhibitory receptor that controls expansion and calcium signaling of the B1 cell population. Nat Immunol 8:695–704. https://doi.org/10.1038/ni1480
134. Morris DL, Rothstein TL. 1993. Abnormal transcription factor induction through the surface immunoglobulin M receptor of B-1 lymphocytes. J Exp Med 177:857–861. https://doi.org/10.1084/jem.177.3.857
135. Sen G, Wu HJ, Bikah G, Venkataraman C, Robertson DA, Snow EC, Bondada S. 2002. Defective CD19-dependent signaling in B-1a and B-1b B lymphocyte subpopulations. Mol Immunol 39:57–68. https://doi.org/10.1016/s0161-5890(02)00047-0
136. Bikah G, Carey J, Ciallella JR, Tarakhovsky A, Bondada S. 1996. CD5-mediated negative regulation of antigen receptor-induced growth signals in B-1 B cells. Science 274:1906–1909. https://doi.org/10.1126/science.274.5294.1906
137. Ochi H, Watanabe T. 2000. Negative regulation of B cell receptor-mediated signaling in B-1 cells through CD5 and Ly49 co-receptors via Lyn kinase activity. Int Immunol 12:1417–1423. https://doi.org/10.1093/intimm/12.10.1417
138. Newman-Rivera AM, Kurzhagen JT, Rabb H. 2022. TCRαβ+ CD4-/CD8- "double negative" T cells in health and disease-implications for the kidney. Kidney Int 102:25–37. https://doi.org/10.1016/j.kint.2022.02.035
139. Brinkman CC, Iwami D, Hritzo MK, Xiong Y, Ahmad S, Simon T, Hippen KL, Blazar BR, Bromberg JS. 2016. Treg engage lymphotoxin beta receptor for afferent lymphatic transendothelial migration. Nat Commun 7:12021. https://doi.org/10.1038/ncomms12021
140. Saxena V, Piao W, Li L, Paluskievicz C, Xiong Y, Simon T, Lakhan R, Brinkman CC, Walden S, Hippen KL, WillsonShirkey M, Lee YS, Wagner C, Blazar BR, Bromberg JS. 2022. Treg tissue stability depends on lymphotoxin beta-receptor- and adenosine-receptor-driven lymphatic endothelial cell responses. Cell Rep 39:110727. https://doi.org/10.1016/j.celrep.2022.110727
141. Ueda Y, Kondo M, Kelsoe G. 2005. Inflammation and the reciprocal production of granulocytes and lymphocytes in bone marrow. J Exp Med 201:1771–1780. https://doi.org/10.1084/jem.20041419
142. Manz MG, Boettcher S. 2014. Emergency granulopoiesis. Nat Rev Immunol 14:302–314. https://doi.org/10.1038/nri3660
143. Moreau JM, Berger A, Nelles ME, Mielnik M, Furlonger C, Cen SY, Besla R, Robbins CS, Paige CJ. 2015. Inflammation rapidly reorganizes mouse bone marrow B cells and their environment in conjunction with early IgM responses. Blood 126:1184–1192. https://doi.org/10.1182/blood-2015-03-635805
144. Bockstal V, Guirnalda P, Caljon G, Goenka R, Telfer JC, Frenkel D, Radwanska M, Magez S, Black SJ. 2011. T. brucei infection reduces B lymphopoiesis in bone marrow and truncates compensatory splenic lymphopoiesis through transitional B-cell apoptosis. PLoS Pathog 7:e1002089. https://doi.org/10.1371/journal.ppat.1002089
145. Bockstal V, Geurts N, Magez S. 2011. Acute disruption of bone marrow B lymphopoiesis and apoptosis of transitional and marginal zone B cells in the spleen following a blood-stage *Plasmodium chabaudi* infection in mice. J Parasitol Res 2011:534697. https://doi.org/10.1155/2011/534697
146. Egawa T, Kawabata K, Kawamoto H, Amada K, Okamoto R, Fujii N, Kishimoto T, Katsura Y, Nagasawa T. 2001. The earliest stages of B cell development require a chemokine stromal cell-derived factor/pre-B cell growth-stimulating factor. Immunity 15:323–334. https://doi.org/10.1016/s1074-7613(01)00185-6
147. Glodek AM, Honczarenko M, Le Y, Campbell JJ, Silberstein LE. 2003. Sustained activation of cell adhesion is a differentially regulated process in B lymphopoiesis. J Exp Med 197:461–473. https://doi.org/10.1084/jem.20021477
148. Tokoyoda K, Egawa T, Sugiyama T, Choi BI, Nagasawa T. 2004. Cellular niches controlling B lymphocyte behavior within bone marrow during

development. Immunity 20:707–718. https://doi.org/10.1016/j.immuni.2004.05.001
149. Pereira JP, An J, Xu Y, Huang Y, Cyster JG. 2009. Cannabinoid receptor 2 mediates the retention of immature B cells in bone marrow sinusoids. Nat Immunol 10:403–411. https://doi.org/10.1038/ni.1710
150. Beck TC, Gomes AC, Cyster JG, Pereira JP. 2014. CXCR4 and a cell-extrinsic mechanism control immature B lymphocyte egress from bone marrow. J Exp Med 211:2567–2581. https://doi.org/10.1084/jem.20140457
151. Griffiths SD, Goodhead DT, Marsden SJ, Wright EG, Krajewski S, Reed JC, Korsmeyer SJ, Greaves M. 1994. Interleukin 7-dependent B lymphocyte precursor cells are ultrasensitive to apoptosis. J Exp Med 179:1789–1797. https://doi.org/10.1084/jem.179.6.1789
152. Gore Y, Starlets D, Maharshak N, Becker-Herman S, Kaneyuki U, Leng L, Bucala R, Shachar I. 2008. Macrophage migration inhibitory factor induces B cell survival by activation of a CD74-CD44 receptor complex. J Biol Chem 283:2784–2792. https://doi.org/10.1074/jbc.M703265200
153. Klasen C, Ziehm T, Huber M, Asare Y, Kapurniotu A, Shachar I, Bernhagen J, El Bounkari O. 2018. LPS-mediated cell surface expression of CD74 promotes the proliferation of B cells in response to MIF. Cell Signal 46:32–42. https://doi.org/10.1016/j.cellsig.2018.02.010
154. Bernhagen J, Krohn R, Lue H, Gregory JL, Zernecke A, Koenen RR, Dewor M, Georgiev I, Schober A, Leng L, Kooistra T, Fingerle-Rowson G, Ghezzi P, Kleemann R, McColl SR, Bucala R, Hickey MJ, Weber C. 2007. MIF is a noncognate ligand of CXC chemokine receptors in inflammatory and atherogenic cell recruitment. Nat Med 13:587–596. https://doi.org/10.1038/nm1567
155. Klasen C, Ohl K, Sternkopf M, Shachar I, Schmitz C, Heussen N, Hobeika E, Levit-Zerdoun E, Tenbrock K, Reth M, Bernhagen J, El Bounkari O. 2014. MIF promotes B cell chemotaxis through the receptors CXCR4 and CD74 and ZAP-70 signaling. J Immunol 192:5273–5284. https://doi.org/10.4049/jimmunol.1302209
156. Stopfer P, Obermeier F, Dunger N, Falk W, Farkas S, Janotta M, Möller A, Männel DN, Hehlgans T. 2004. Blocking lymphotoxin-beta receptor activation diminishes inflammation via reduced mucosal addressin cell adhesion molecule-1 (MAdCAM-1) expression and leucocyte margination in chronic DSS-induced colitis. Clin Exp Immunol 136:21–29. https://doi.org/10.1111/j.1365-2249.2004.02402.x
157. Matsumoto M, Lo SF, Carruthers CJL, Min J, Mariathasan S, Huang G, Plas DR, Martin SM, Geha RS, Nahm MH, Chaplin DD. 1996. Affinity maturation without germinal centres in lymphotoxin-α-deficient mice. Nature 382:462–466. https://doi.org/10.1038/382462a0
158. Bortnick A, Chernova I, Quinn WJ III, Mugnier M, Cancro MP, Allman D. 2012. Long-lived bone marrow plasma cells are induced early in response to T cell-independent or T cell-dependent antigens. J Immunol 188:5389–5396. https://doi.org/10.4049/jimmunol.1102808
159. Spahn TW, Kucharzik T. 2004. Modulating the intestinal immune system: the role of lymphotoxin and GALT organs. Gut 53:456–465. https://doi.org/10.1136/gut.2003.023671
160. Reboldi A, Arnon TI, Rodda LB, Atakilit A, Sheppard D, Cyster JG. 2016. IgA production requires B cell interaction with subepithelial dendritic cells in Peyer's patches. Science 352:aaf4822. https://doi.org/10.1126/science.aaf4822
161. Li C, Lam E, Perez-Shibayama C, Ward LA, Zhang J, Lee D, Nguyen A, Ahmed M, Brownlie E, Korneev KV, Rojas O, Sun T, Navarre W, He HH, Liao S, Martin A, Ludewig B, Gommerman JL. 2019. Early-life programming of mesenteric lymph node stromal cell identity by the lymphotoxin pathway regulates adult mucosal immunity. Sci Immunol 4. https://doi.org/10.1126/sciimmunol.aax1027
162. Pabst O. 2012. New concepts in the generation and functions of IgA. Nat Rev Immunol 12:821–832. https://doi.org/10.1038/nri3322
163. Merino MC, Montes CL, Acosta-Rodriguez EV, Bermejo DA, Amezcua-Vesely MC, Gruppi A. 2010. Peritoneum from *Trypanosoma cruzi*-infected mice is a homing site of Syndecan-1 neg plasma cells which mainly provide non-parasite-specific antibodies. Int Immunol 22:399–410. https://doi.org/10.1093/intimm/dxq019
164. Gunn MD, Ngo VN, Ansel KM, Ekland EH, Cyster JG, Williams LT. 1998. A B-cell-homing chemokine made in lymphoid follicles activates Burkitt's lymphoma receptor-1. Nature 391:799–803. https://doi.org/10.1038/35876
165. Cyster JG, Ansel KM, Reif K, Ekland EH, Hyman PL, Tang HL, Luther SA, Ngo VN. 2000. Follicular stromal cells and lymphocyte homing to follicles. Immunol Rev 176:181–193. https://doi.org/10.1034/j.1600-065x.2000.00618.x
166. Suto H, Katakai T, Sugai M, Kinashi T, Shimizu A. 2009. CXCL13 production by an established lymph node stromal cell line via lymphotoxin-beta receptor engagement involves the cooperation of multiple signaling pathways. Int Immunol 21:467–476. https://doi.org/10.1093/intimm/dxp014
167. Carlsen HS, Baekkevold ES, Morton HC, Haraldsen G, Brandtzaeg P. 2004. Monocyte-like and mature macrophages produce CXCL13 (B cell-attracting chemokine 1) in inflammatory lesions with lymphoid neogenesis. Blood 104:3021–3027. https://doi.org/10.1182/blood-2004-02-0701
168. Louwe PA, Badiola Gomez L, Webster H, Perona-Wright G, Bain CC, Forbes SJ, Jenkins SJ. 2021. Recruited macrophages that colonize the post-inflammatory peritoneal niche convert into functionally divergent resident cells. Nat Commun 12:1770. https://doi.org/10.1038/s41467-021-21778-0
169. Askenase MH, Han S-J, Byrd AL, Morais da Fonseca D, Bouladoux N, Wilhelm C, Konkel JE, Hand TW, Lacerda-Queiroz N, Su X, Trinchieri G, Grainger JR, Belkaid Y. 2015. Bone-marrow-resident NK cells prime monocytes for regulatory function during infection. Immunity 42:1130–1142. https://doi.org/10.1016/j.immuni.2015.05.011
170. Wijdeven RH, van Luijn MM, Wierenga-Wolf AF, Akkermans JJ, van den Elsen PJ, Hintzen RQ, Neefjes J. 2018. Chemical and genetic control of IFNγ-induced MHCII expression. EMBO Rep 19:e45553. https://doi.org/10.15252/embr.201745553
171. Sorg UR, Behnke K, Degrandi D, Reich M, Keitel V, Herebian D, Deenen R, Beyer M, Schultze JL, Köhrer K, Gabbert HE, Mayatepek E, Häussinger D, Pfeffer K. 2016. Cooperative role of lymphotoxin β receptor and tumor necrosis factor receptor p55 in murine liver regeneration. J Hepatol 64:1108–1117. https://doi.org/10.1016/j.jhep.2015.12.006
172. De Trez C, Ware CF. 2008. The TNF receptor and Ig superfamily members form an integrated signaling circuit controlling dendritic cell homeostasis. Cytokine Growth Factor Rev 19:277–284. https://doi.org/10.1016/j.cytogfr.2008.04.013
173. Remouchamps C, Boutaffala L, Ganeff C, Dejardin E. 2011. Biology and signal transduction pathways of the Lymphotoxin-αβ/LTβR system. Cytokine Growth Factor Rev 22:301–310. https://doi.org/10.1016/j.cytogfr.2011.11.007
174. Albarbar B, Dunnill C, Georgopoulos NT. 2015. Regulation of cell fate by lymphotoxin (LT) receptor signalling: functional differences and similarities of the LT system to other TNF superfamily (TNFSF) members. Cytokine Growth Factor Rev 26:659–671. https://doi.org/10.1016/j.cytogfr.2015.05.001
175. Smith T, Heger A, Sudbery I. 2017. UMI-tools: modeling sequencing errors in Unique Molecular Identifiers to improve quantification accuracy. Genome Res 27:491–499. https://doi.org/10.1101/gr.209601.116
176. Martin M. 2011. Cutadapt removes adapter sequences from high-throughput sequencing reads. EMBnet J 17:10–12. https://doi.org/10.14806/ej.17.1.200
177. Kopylova E, Noé L, Touzet H. 2012. SortMeRNA: fast and accurate filtering of ribosomal RNAs in metatranscriptomic data. Bioinformatics 28:3211–3217. https://doi.org/10.1093/bioinformatics/bts611
178. Dobin A, Davis CA, Schlesinger F, Drenkow J, Zaleski C, Jha S, Batut P, Chaisson M, Gingeras TR. 2013. STAR: ultrafast universal RNA-seq aligner. Bioinformatics 29:15–21. https://doi.org/10.1093/bioinformatics/bts635
179. Danecek P, Bonfield JK, Liddle J, Marshall J, Ohan V, Pollard MO, Whitwham A, Keane T, McCarthy SA, Davies RM, Li H. 2021. Twelve years of SAMtools and BCFtools. Gigascience 10. https://doi.org/10.1093/gigascience/giab008
180. Liao Y, Smyth GK, Shi W. 2014. featureCounts: an efficient general purpose program for assigning sequence reads to genomic features. Bioinformatics 30:923–930. https://doi.org/10.1093/bioinformatics/btt656
181. Love MI, Huber W, Anders S. 2014. Moderated estimation of fold change and dispersion for RNA-seq data with DESeq2. Genome Biol 15:550. https://doi.org/10.1186/s13059-014-0550-8
182. Korotkevich G, Sukhov V, Budin N, Shpak B, Artyomov MN, Sergushichev A. 2016. Fast gene set enrichment analysis. bioRxiv. https://doi.org/10.1101/060012